Electronic Supplementary Material (ESI) for Journal of Materials Chemistry A.

Calixarene-based Porous 3D Polymers and Copolymers with High Capacity and Binding Energy for CO_2, CH_4 and Xe Capture

*A. Pedrini, J. Perego, S. Bracco, C. X. Bezuidenhout, P. Sozzani and A. Comotti**

University of Milano Bicocca, Department of Materials Science, Via R. Cozzi 55,
20125 Milan, Italy

Index

1 General experimental methods

Synthesis

Unless stated otherwise, reactions were conducted in flame-dried glassware under nitrogen atmosphere using anhydrous solvents (either freshly distilled or passed through activated alumina columns). All commercially obtained reagents were used as received unless otherwise specified.

Solution NMR spectroscopy

NMR spectra were obtained using a Bruker Ascend 400 (400 MHz) spectrometer at 25 °C. ^{1}H NMR chemical shifts (δ) were reported in ppm relative to the proton resonances resulting from incomplete deuteration of the NMR solvents.

Solid state NMR spectroscopy

^{13}C solid-state NMR experiments were carried out with a Bruker Avance 300 instrument operating at a static field of 7.04 T equipped with high-power amplifiers (1 kW) and a 4 mm double resonance MAS probe. ^{13}C{^{1}H} ramped-amplitude cross polarization (CP) experiments were performed at a spinning speed of 12.5 kHz using a recycle delay of 5 s and a contact time of 2 ms. The 90° pulse for proton was 2.9 μs. Crystalline polyethylene was taken as an external reference at 32.8 ppm from TMS.

IR spectroscopy

IR spectra were acquired by ATR method by means of a Nicolet iS10 instrument over the range 4000-600 cm^{-1}. In the following, signal intensities are denoted as br = broad, vs = very strong, s = strong, m = medium, and w = weak.

Powder X-ray diffraction spectroscopy (PXRD)

Samples were ground with agate mortar and pestle and deposited in the hollow of glass sample-holder. Diffraction data were collected at room temperature on a Rigaku Miniflex 600 diffractometer operated with Cu$_{K\alpha 1}$ radiation (λ = 1.54060 Å). The generator was set at 40 kV and 15 mA. Acquisitions were performed in the 3 - 50° 2θ range, with steps of 0.02°, and speed of 0.8 s/step.

Differential scanning calorimetry (DSC)

Measurements were performed on a Mettler-Toledo StarE instrument from 25 to 400 °C or from 25 to 450 °C, at a heating rate of 10 °C/min and under a 80 mL/min flow of N_2.

Thermogravimetric Analyses (TGA)

Measurements were performed on a Mettler- Toledo DSC/TGA 1 StarE System from 0 to 800 °C at a 10 °C/min heating rate under a 50 ml/min flux of air.

Scanning Electron Microscopy

Scanning electron microscopy (SEM) images were collected using Zeiss Gemini 500 scanning electron microscopy, operating at 10 kV.

Helium Pycnometry

Helium pycnometer analyses were performed with a Micromeritics AccuPyc II 1340 Pycnometer with a 1 cm^3 sample holder. The samples were previously treated in vacuum at 120 °C for 4 h. Five independent measurements were collected for each sample and averaged to minimize errors.

Gas adsorption measurements

All adsorption and breakthrough experiments were performed using gases with minimum purity of 5.0 (N_2, He and CH_4) and 4.5 (CO_2). N_2 adsorption isotherms at 77 K were collected on a Micromeritics ASAP 2020 instrument, the samples were treated overnight at 150 °C under vacuum. The surface area was calculated from the N_2 adsorption isotherm at 77 K using the data in the pressure range $p/p°$ from 0.015 to 0.1, according to the Brunauer-Emmett-Teller (BET) and Langmuir models. The total pore volume was calculated from the N_2 adsorption isotherms at 77 K by the NLDFT method with the carbon slit pore model up to $p/p°$ 0.98. The microporosity was calculated at $p/p° = 0.1$.
CO_2, CH_4 and N_2 adsorption isotherms at 298, 283 and 273 K and up to 10 bar were collected on a Micromeritics ASAP 2050 instrument, the temperature was controlled using a Julabo F12-ED refrigerated/heating circulator.

Adsorption coupled to microcalorimetry

A volumetric adsorption analyzer (Micromeritics ASAP 2050) was coupled with a Setaram μDSC7 Evo instrument equipped with a high pressure sample holder. The set-up allowed simultaneous determination of CO_2 adsorption isotherms and heat exchanged during the adsorption process at each adsorption step. Sorption-coupled microcalorimetry measurements were performed three times at 293 K and the three different runs were averaged to reduce experimental errors.

Column breakthrough measurements

Dynamic breakthrough measurements were performed on a Micromeritics selective adsorption analyzer (SAA) equipped with He, N_2 and CO_2 gases. The outlet gas flow was monitored with a Pfeiffer vacuum ThermoStar gas analysis system.

Sample **CXF1-OH** (101.7 mg) was degassed under high vacuum at 100°C to remove adsorbed moisture, cooled to room temperature and quickly loaded in the ¼" stainless steel column of SAA analyzer with a small amount of cotton wool. The column was gently tapped to ensure proper packing of the powdery material and mounted on the breakthrough apparatus under nitrogen flow. Blank runs were performed under the same experimental conditions by loading the column with a similar volume of glass beads and cotton wool.

The sample was flushed with nitrogen at a total flow rate of 20 standard cubic centimeter *per* minutes (sccm) for at least 3 hours before performing a breakthrough experiment. The experiments were performed with a constant flow rate of 4 sccm using nitrogen as carrier gas and switching to CO_2/N_2 mixtures (15/85 or 5/95) to investigate the separation properties of the material while maintaining a total flow rate of 4 sccm. At the end of the breakthrough experiment, the column saturated with CO_2 was regenerated by flowing nitrogen (20 sccm) at 298 K.

Solid State NMR: ^{1}H, ^{13}C and Hyperpolarized ^{129}Xe NMR

^{13}C and ^{1}H solid-state NMR experiments were carried out with a Bruker Avance 300 instrument operating at a static field of 7.04 T equipped with high-power amplifiers (1 kW) and a 4 mm double resonance MAS probe. $^{13}C\{^1H\}$ ramped-amplitude Cross Polarization (CP) experiments were performed at a spinning speed of 12.5 kHz using a recycle delay of 5 s and contact time of 2 ms and 0.05 ms. The 90° pulse for proton was 2.5 μs. Crystalline polyethylene was taken as an external reference at 32.8 ppm from TMS. Quantitative solid-state ^{13}C MAS NMR spectra (single-pulse excitation SPE) were performed at a spinning speed of 12.5 kHz using a recycle delay of 100 s. ^{1}H MAS NMR spectra (single-pulse excitation SPE) were performed at a spinning speed of 12.5 kHz using a recycle delay of 20 s. The ^{1}H chemical shift was referenced to adamantane.

Hyperpolarization ^{129}Xe NMR experiments were performed by a home-built apparatus with a continuous-flow delivery of hyperpolarized xenon gas with a Bruker Avance 300 spectrometer operating at a Larmor Frequency of 83.02 MHz for ^{129}Xe. A diode array laser delivering 6 W at 795 nm was applied, circular polarization was achieved using a beam splitting cube and quarter wave plate. A stream of gas mixture containing 2% xenon, 2% nitrogen and 96% helium at 2 atm was used and the gas flow rate was maintained at 20 L/h. The samples were outgassed overnight at 120°C in vacuum, then were pressed in a glass tube before being inserted into the coil. A pulse duration of 7 μs was applied, with a recycle delay of 0.5 s. Variable temperatures experiments in the range 298 - 212 K were achieved by flowing cooled nitrogen gas around the sample region. The ^{129}Xe NMR chemical shifts were referenced to xenon gas set at 0 ppm.

2 Synthetic procedures

2.1 Synthesis of tetrabrominated calixarenes

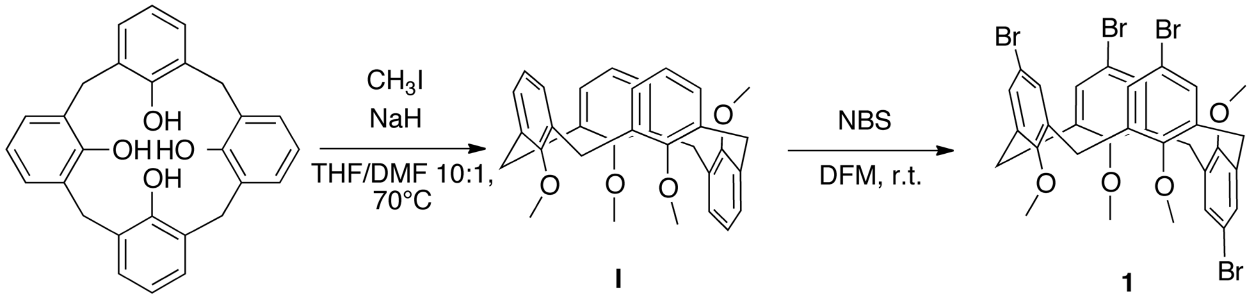

Scheme S1. Synthesis of 5,11,17,23-tetrabromo-25,26,27,28-tetramethoxy-calix[4]arene (**CX1**).

25,26,27,28-Tetramethoxy-calix[4]arene (I) was synthesized according to a slightly modified reported procedure.[1] NaH (60% dispersion in mineral oil, 1.13 g, 28.3 mmol) was added to a solution of 25,26,27,28-tetrahydroxycalix[4]arene (1.2 g, 2.8 mmol) in a 10:1 mixture of tetrahydrofuran (THF)/ *N*,*N*-dimethylformamide (DMF) and the mixture was stirred at r.t. under nitrogen flux for 30 min. Iodomethane (1.8 mL, 28.3 mmol) was added and the mixture was heated at 70 °C overnight. After cooling at room temperature, MeOH (10 mL) was added and the mixture was stirred for 30 min. Volatiles were removed under reduced pressure and the deep yellow residue was partitioned between CH_2Cl_2 (60 mL) and water (60 mL). The aqueous phase was extracted with 40 mL of CH_2Cl_2 and the organics were combined, washed with water (100 mL) and dried on Na_2SO_4. After the removal of the solvent under reduced pressure, the crude was purified by recrystallization form CH_2Cl_2/MeOH mixture affording compound **I** as a white solid (1.23 g, 2.3 mmol, 82% yield). ^{1}H NMR ($CDCl_3$, 400 MHz, 298 K): δ = 7.2-6.3 (bm, 12H, Ar**H**), 4.5-2.9 (bm, 20H, ArC$\mathbf{H_2}$ and OC$\mathbf{H_3}$); IR (ATR, cm^{-1}): 2928 (m), 2816 (w), 1460 (s), 1424 (s), 1245 (s), 1203 (s), 1169 (m), 1087 (s), 1019 (vs), 1009 (vs), 817 (w), 770 (vs), 610 (m).

5,11,17,23-Tetrabromo-25,26,27,28-tetramethoxy-calix[4]arene (CX1) was synthesized adapting a published procedure.[2] Compound **I** (0.35 g, 0.73 mmol) was dissolved in 12 mL of DMF and *N*-bromosuccinimide (1.14 g, 6.4 mmol) was added. The mixture was stirred at room temperature for 24 h. An aqueous 1 M solution of HCl (40 mL) was slowly added and the yellow precipitate was filtered, washed with water and dried. Recrystallization from MeOH afforded pure compound **CX1** as a white powder (0.51 g, 0.64 mmol, 88% yield). ^{1}H NMR ($CDCl_3$, 400 MHz, 298 K): δ = 7.37 (s, 2H, Ar$\mathbf{H_8}$), 7.22 (s, 2H, Ar$\mathbf{H_3}$), 7.08 (s, 2H, Ar$\mathbf{H_5}$), 6.87 (s, Ar$\mathbf{H_{cone}}$), 6.53 (s, 2H, Ar$\mathbf{H_4}$), 4.26 (d, J = 13.4 Hz, ArC$\mathbf{H_{cone}}$), 3.99 (d, J = 13.8 Hz, 2H, ArC$\mathbf{H_5}$), 3.78 (s, OC$\mathbf{H_{cone}}$), 3.68 (m, 9H, OC$\mathbf{H_{II+III}}$), 3.53 (m, 4H, ArC**H**$_{6,7}$), 3.12 (d, J = 13.4 Hz, ArC**H**$_{\mathrm{cone}}$), 3.06 (m, 5H, OC**H**$_{\mathrm{I}}$ + ArC**H**$_2$), for signal assignment see reference 3; ^{13}C NMR (CDCl$_3$, 100 MHz, 298 K): δ = 157.0, 156.3, 138.1, 136.4, 135.1, 133.1, 131.8, 131.0, 130.8, 115.6, 115.5, 115.1, 114.4, 61.8, 61.1, 60.0, 59.4, 34.9, 30.2, 30.1; IR (ATR, cm^{-1}): 2927 (m), 2816 (w), 1458 (s), 1424 (s), 1245 (s), 1202 (vs), 1169 (m), 1086 (s), 1078 (s), 1018 (vs), 1009 (vs), 828 (w), 817 (m), 770 (vs= 618 (m), 610 (s).

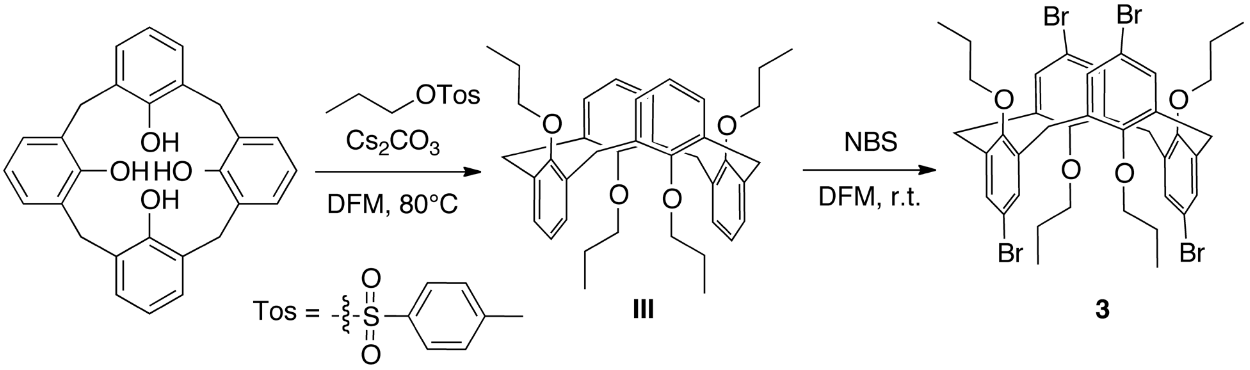

Scheme S2. Synthesis of 5,11,17,23-tetrabromo-25,26,27,28-tetrapropoxy-calix[4]arene in 1,3-alternate conformer (**CX2**).

25,26,27,28-Tetrapropoxy-calix[4]arene (1,3-alternate conformer) (II) was synthesized according to a slightly modified reported procedure.[5] A mixture of 25,26,27,28-tetrahydroxycalix[4]arene (1.2 g, 2.8 mmol) and Cs$_2$CO$_3$ (6.9 g, 21.2 mmol) in DMF (60 mL) was heated at 80 °C for 30 min. *n*-Propyl tosylate (3.95 mL, 21.2 mmol) was added dropwise the temperature was maintained for 6 h. The mixture was cooled to room temperature, poured onto water (400 mL) and extracted with dichloromethane (3 x 200 mL). The combined organic extracts were washed with 1 N HCl (200 mL) and brine (200 mL), dried over anhydrous sodium sulfate and evaporated under reduced pressure. The resulting crude solid was recrystallized twice from a CH$_2$Cl$_2$/MeOH mixture affording compound **II** as white needles (0.69 g, 1.2 mmol, 41% yield). ^{1}H NMR (CDCl$_3$, 400 MHz, 298 K): δ = 6.99 (d, J = 7.6 Hz, 8H, Ar**H**), 6.67 (t, J = 7.6 Hz, 4H, Ar**H**), 3.61 (s, 8H, ArC**H**$_2$), 3.53 (t, J = 7.2 Hz, 8H, OC**H**$_2$), 1.63 (m, 8H, -C**H**$_2$-), 0.92 (t, J = 7.6 Hz, 12H, C**H**$_3$); IR (ATR, cm^{-1}): 2959 (w), 2933 (m), 2873 (w), 1449 (s), 1386 (m), 1245 (s), 1192 (vs), 1087 (s), 1043 (s), 1007 (vs), 963 (s), 761 (vs), 622 (s).

5,11,17,23-tetrabromo-25,26,27,28-tetrapropoxy-calix[4]arene (1,3-alternate conformer) (CX2) was synthesized according to a published procedure.[2] Compound **II** (0.35 g, 0.6 mmol) was dissolved in 25 mL of DMF and *N*-bromosuccinimide (0.92 g, 5.2 mmol) was added. The mixture was stirred at room temperature for 24 h. An aqueous 1 M solution of HCl (40 mL) was slowly added and the yellow precipitate was filtered, washed with water and dried. Recrystallization from CH_2Cl_2/MeOH afforded pure compound **CX2** as white needles (0.42 g, 0.46 mmol, 76% yield). ^{1}H NMR ($CDCl_3$, 400 MHz, 298 K): δ = 7.15 (s, 8H, Ar**H**), 3.54 (m, 16H, ArC**H₂** + OC**H₂**), 1.65 (m, 8H, -C**H₂**-), 0.99 (t, J = 7.6 Hz, 12H, C**H₃**); ^{13}C NMR ($CDCl_3$, 100 MHz, 298 K): δ = 155.5, 134.9, 132.6, 114.5, 73.4, 36.1, 23.4, 10.5; IR (ATR, cm^{-1}): 2960 (w), 2963 (m), 2874 (w), 1575 (w), 1448 (s), 1383 (m), 1255 (w), 1194 (vs), 1064 (s), 1005 (s), 954 (vs), 856 (s), 792 (w), 759 (w).

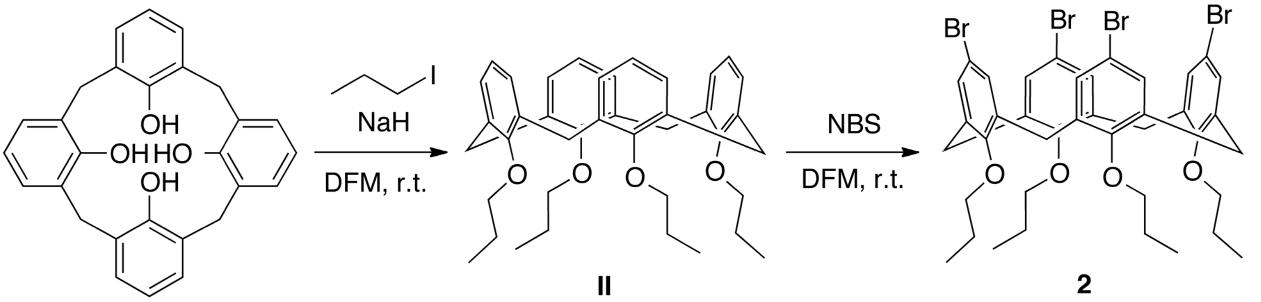

Scheme S3. Synthesis of 5,11,17,23-tetrabromo-25,26,27,28-tetrapropoxy-calix[4]arene as cone conformer (**CX3**).

25,26,27,28-Tetrapropoxy-calix[4]arene (cone conformer) (III) was synthesized according to a slightly modified reported procedure.[4] NaH (60% dispersion in mineral oil, 0.47 g, 11.7 mmol) was added to a solution of 25,26,27,28-tetrahydroxycalix[4]arene (0.5 g, 1.2 mmol) in 10 mL of DMF and the mixture was stirred at r.t. under nitrogen flux for 30 min. 1-Iodopropane (1.14 mL, 11.7 mmol) was added an the mixture was stirred at r.t. for 12 h. An aqueous 2 M solution of HCl (20 mL) was slowly added and the precipitate was filtered, washed with water and dried. The crude was purified by recrystallization form MeOH mixture affording compound **III** as a white solid (0.55 g, 0.9 mmol, 80% yield). ^{1}H NMR ($CDCl_3$, 400 MHz, 298 K): δ = 6.62 (m, 12H, Ar**H**), 4.47 (d, J = 13.3 Hz, 4H, ArC**H$_{ax}$**), 3.87 (m, 8H, OC**H₂**), 3.17 (d, J = 13.3 Hz, 4H, ArC**H$_{eq}$**), 1.95 (m, 8H, -C**H₂**-), 1.01 (t, J = 7.5 Hz, 12H, C**H₃**); IR (ATR, cm^{-1}): 2961 (m), 2922 (m), 2872 (m), 1584 (w), 1454 (s), 1381 (m), 1291 (w), 1244 (w), 1208 (s), 1190 (s), 1088 (s), 1065 (w), 1041 (m), 1007 (s), 965 (s), 762 (vs), 625 (s).

5,11,17,23-tetrabromo-25,26,27,28-tetrapropoxy-calix[4]arene (cone conformer) (CX3) was synthesized according to a published procedure.[2] Compound **III** (0.55 g, 0.93 mmol) was dissolved in 20 mL of DMF and *N*-bromosuccinimide (1.45 g, 8.16 mmol) was added. The mixture was stirred at room temperature for 24 h. An aqueous 1 M solution of HCl (60 mL) was slowly added and the yellow precipitate was filtered, washed with water and dried. Recrystallization from CH_2Cl_2/MeOH afforded pure compound **CX3** as a white powder (0.65 g, 0.71 mmol, 76% yield). ^{1}H NMR ($CDCl_3$, 400 MHz, 298 K): δ = 6.80 (s, 8H, Ar**H**), 4.35 (d, J = 13.4 Hz, 4H, ArC**H$_{ax}$**), 3.80 (m, 8H, OC**H$_2$**), 3.07 (d, J = 13.5 Hz, 4H, ArC**H$_{eq}$**), 1.86 (m, 8H, -C**H$_2$**-), 0.97 (t, J = 7.5 Hz, 12H, C**H$_3$**); ^{13}C NMR ($CDCl_3$, 100 MHz, 298 K): δ = 155.5, 136.4, 131.0, 115.1, 77.0, 30.7, 23.1, 10.2; IR (ATR, cm^{-1}): 2962 (m), 2925 (m), 2872 (m), 1569 (m), 1455 (s), 1387 (m), 1293 (w), 1250 (w), 1197 (vs), 1067 (w), 1038 (w), 1000 (s), 962 (s), 848 (vs), 620 (w).

2.2 Frameworks synthesis

Homopolymeration reaction. The catalytic mixture was prepared by adding *cis*,*cis*-1,5-cyclooctadiene (0.25 mL), 2,2'bypiridyl (0.25 g) and $Ni(COD)_2$ (0.5 g, 1.89 mmol) to a mixture of freshly distilled DMF (45 mL) and THF (15 mL). After stirring at 0°C for 15 minutes, a solution of calix[4]arene **CX1-CX3** (0.31 mmol) in THF (15 mL) was added dropwise to the deep-purple solution of the catalyst and the resulting mixture was stirred at room temperature for 48 h. The reaction was then quenched by adding aqueous 1 M HCl (30 mL), until the suspension turned green. The off-white precipitate was filtered and washed with THF (3 x 30 mL), water (3 x 30 mL) and chloroform (3 x 30 mL) and dried under vacuum at 150°C.

Copolymerization reaction. The catalytic mixture was prepared by adding *cis*,*cis*-1,5-cyclooctadiene (0.1 mL), 2,2'bypiridyl (0.1 g) and $Ni(COD)_2$ (2.0 g, 7.27 mmol) to a mixture of freshly distilled DMF (180 mL) and THF (60 mL). After stirring at 0°C for 15 minutes, a solution of calix[4]arene **CX3** (0.286 g, 0.31 mmol) and tetrakis(4-bromophenyl)methane (0.800 g, 1.26 mmol) in THF (60 mL) was added dropwise to the deep-purple solution of the catalyst and the resulting mixture was stirred at room temperature for 48 h. The reaction was then quenched by adding aqueous 1 M HCl (120 mL), until the suspension turned green. The white precipitate was filtered and washed with THF (3 x 50 mL), water (3 x 50 mL) and chloroform (3 x 50 mL) and dried under vacuum at 150°C.

General dealkylation reaction. The alkylated frameworks **CXF1-OMe**, **CXF2-OPr** and **co-CXF3-OPr** (0.15 g) was dispersed in 2 mL of BBr_3 and the mixture was degassed (3 x freeze-pump-thaw) and stirred at room temperature for 24 h. The volatiles were removed under reduced pressure and the solid was washed with CH_2Cl_2 (3 x 50 mL), acetone (3 x 50 mL) and water (3 x 50 mL) to afford the dealkylated framework as a tan powder that was dried under vacuum at 150 °C.

3 NMR Spectra in solution

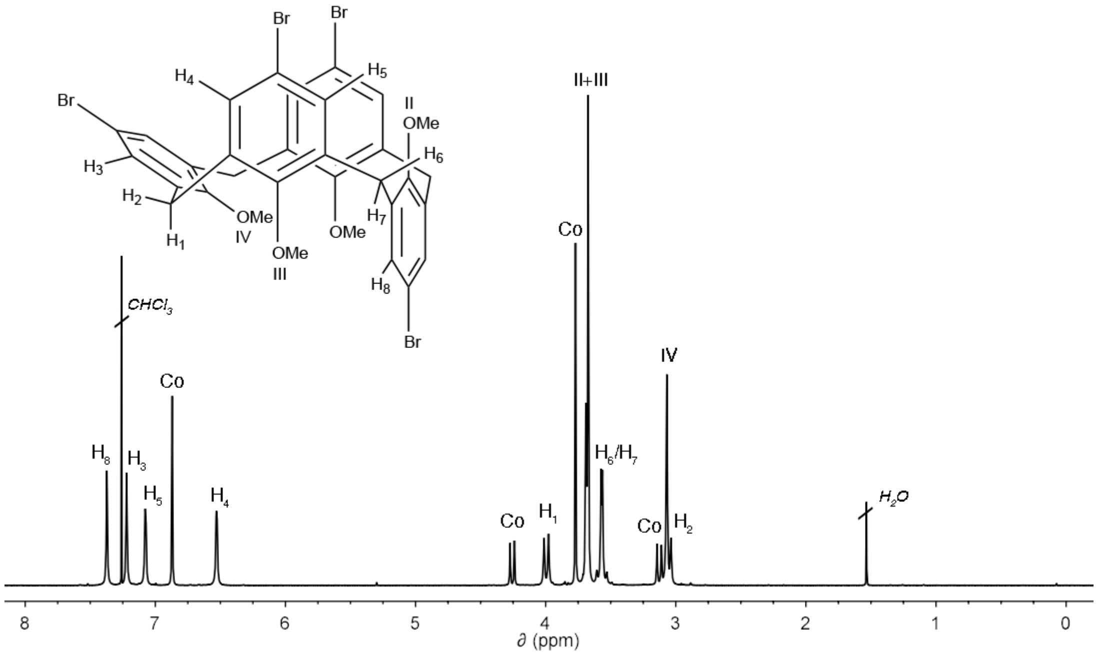

Figure S1. ^{1}H NMR spectrum ($CDCl_3$, 400 MHz, 298 K) of 5,11,17,23-tetrabromo-25,26,27,28-tetramethoxy-calix[4]arene (**CX1**).

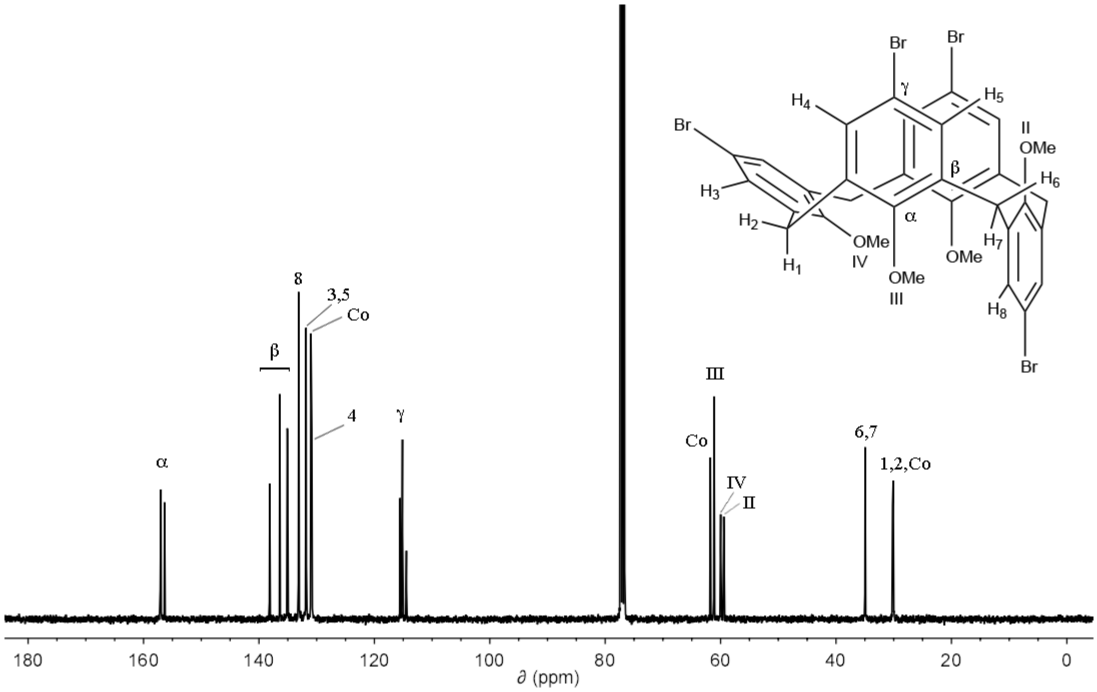

Figure S2. $^{13}C\{^1H\}$ NMR spectrum ($CDCl_3$, 100 MHz, 298 K) of 5,11,17,23-tetrabromo-25,26,27,28-tetramethoxy-calix[4]arene (**CX1**).

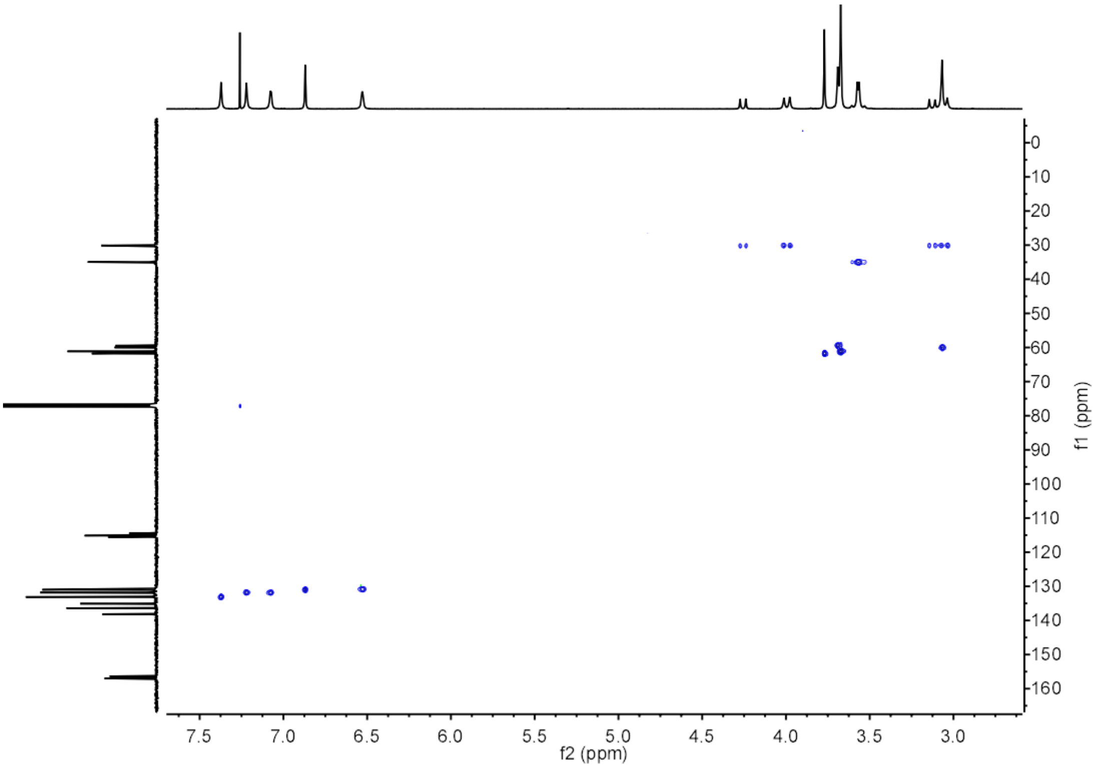

Figure S3. ^{1}H-^{13}C HSQC (400 MHz, $CDCl_3$, 297 K) spectrum of 5,11,17,23-tetrabromo-25,26,27,28-tetramethoxy-calix[4]arene (**CX1**).

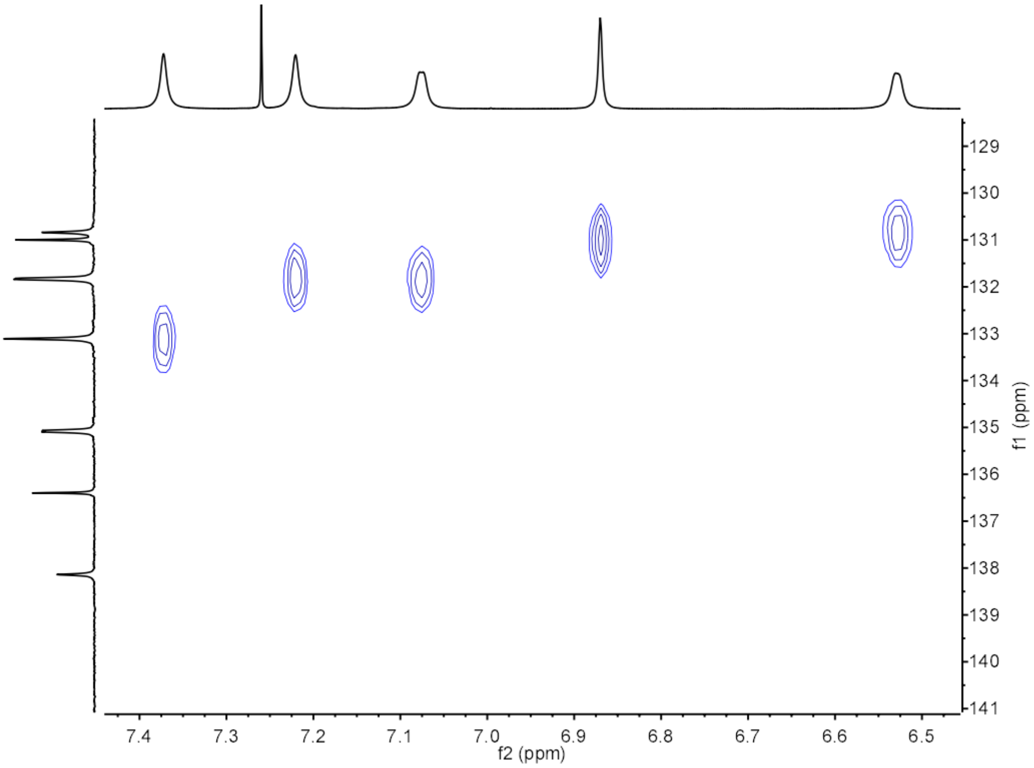

Figure S4. Aromatic region of ^{1}H-^{13}C HSQC (400 MHz, $CDCl_3$, 297 K) spectrum of 5,11,17,23-tetrabromo-25,26,27,28-tetramethoxy-calix[4]arene (**CX1**).

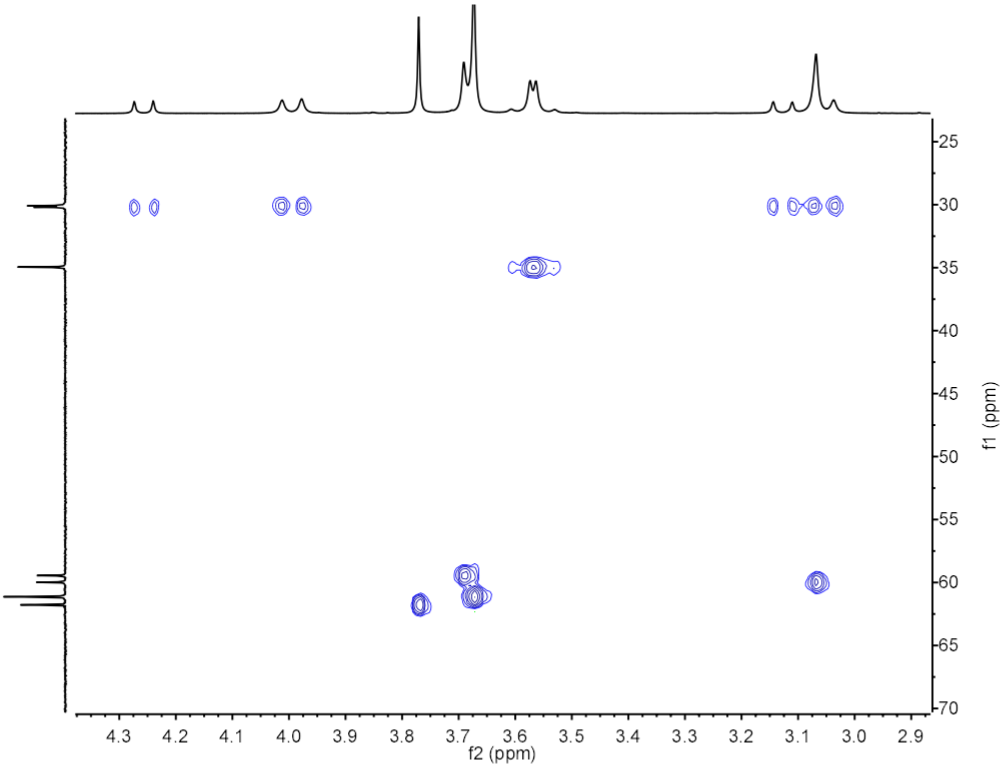

Figure S5. Aliphatic region of ^{1}H-^{13}C HSQC (400 MHz, CDCl$_3$, 297 K) spectrum of 5,11,17,23-tetrabromo-25,26,27,28-tetramethoxy-calix[4]arene (**CX1**).

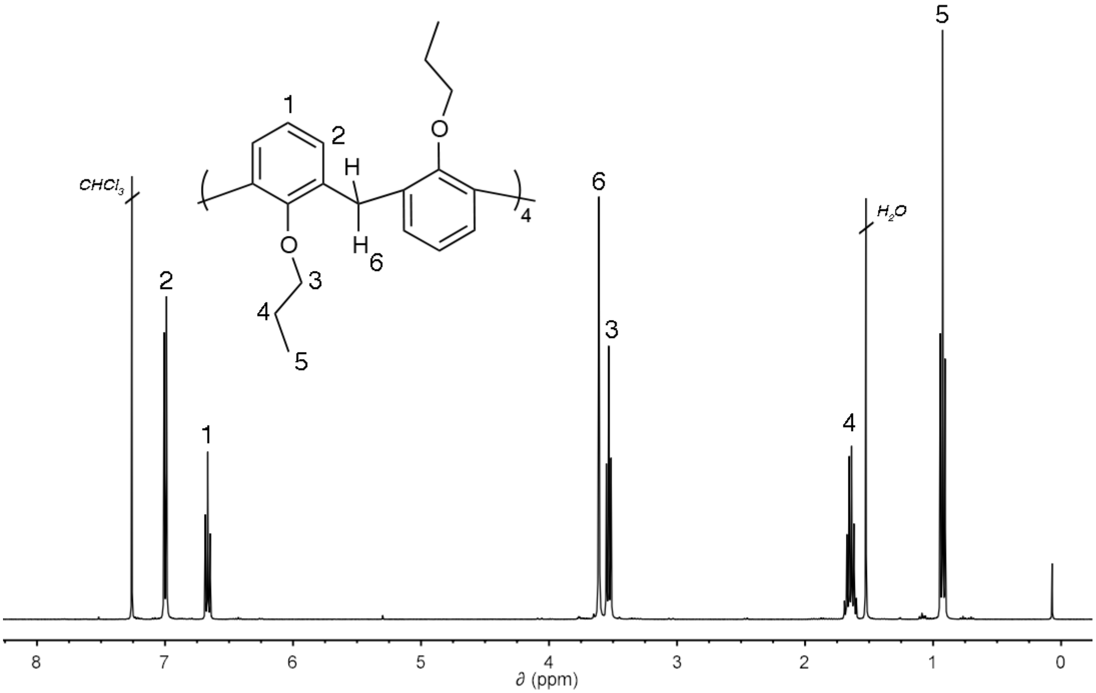

Figure S6. ^{1}H NMR spectrum (CDCl$_3$, 400 MHz, 298 K) of compound **II**.

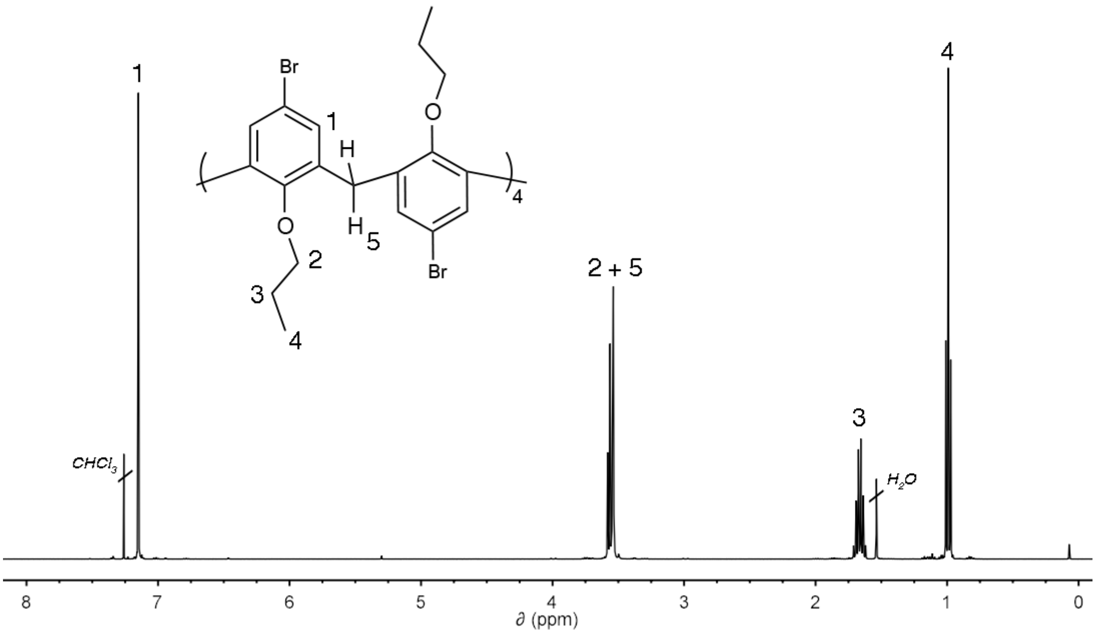

Figure S7. ^{1}H NMR spectrum ($CDCl_3$, 400 MHz, 298 K) of 5,11,17,23-tetrabromo-25,26,27,28-tetrapropoxy-calix[4]arene (**CX2**).

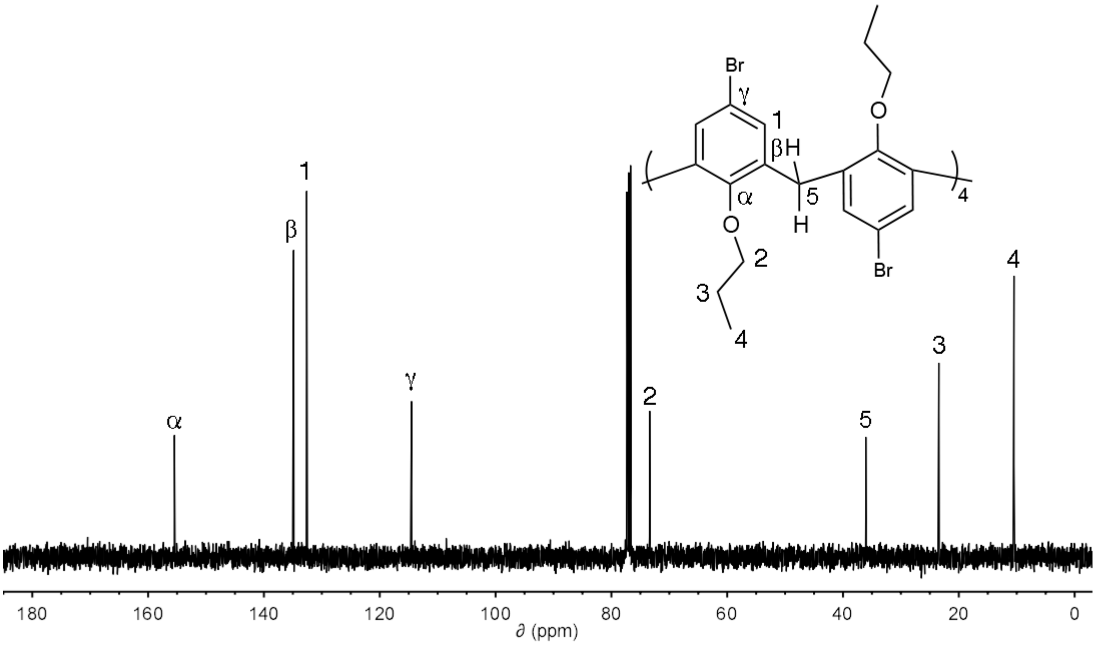

Figure S8. $^{13}C\{^{1}H\}$ NMR spectrum ($CDCl_3$, 100 MHz, 298 K) of 5,11,17,23-tetrabromo-25,26,27,28-tetrapropoxy-calix[4]arene (**CX2**).

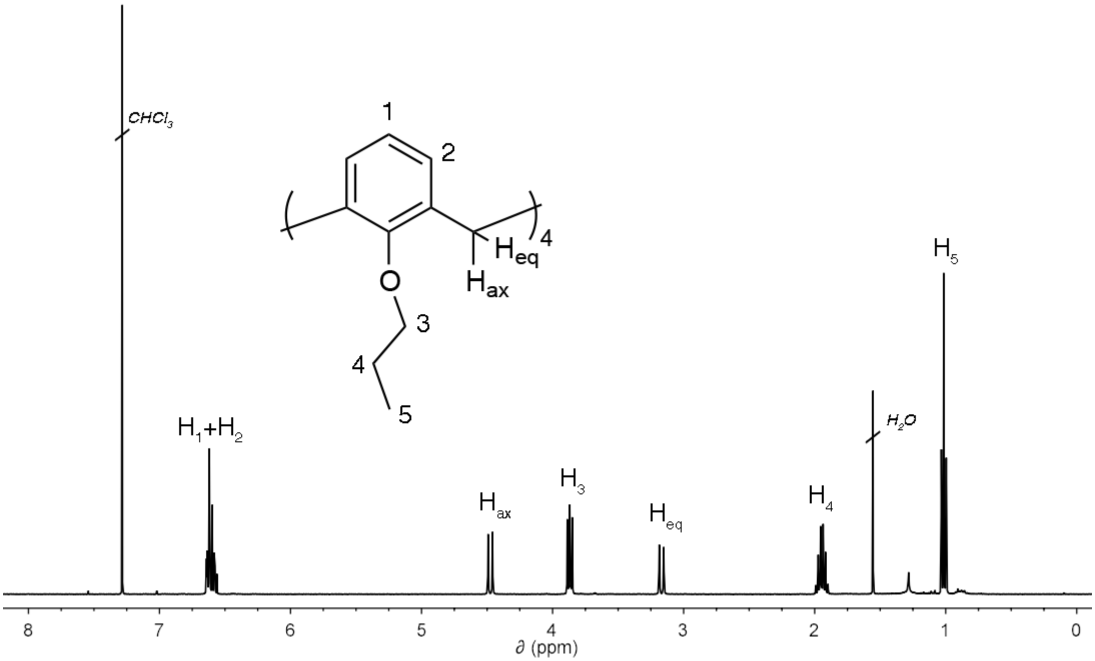

Figure S9. ^{1}H NMR spectrum ($CDCl_3$, 400 MHz, 298 K) of compound **III**.

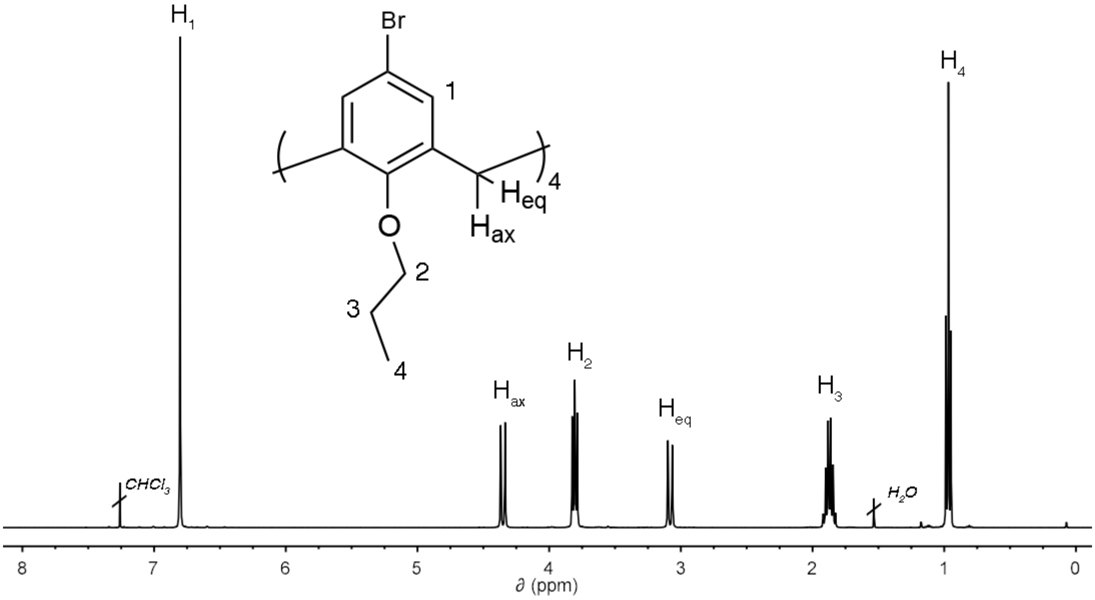

Figure S10. ^{1}H NMR spectrum ($CDCl_3$, 400 MHz, 298 K) of 5,11,17,23-tetrabromo-25,26,27,28-tetrapropoxy-calix[4]arene (**CX3**).

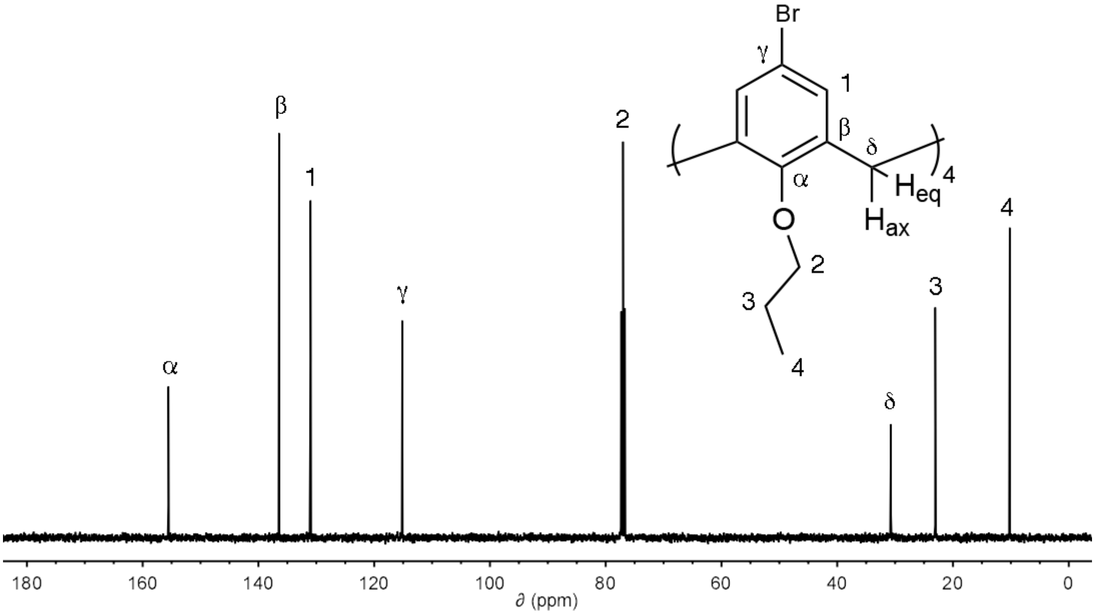

Figure S11. $^{13}C\{^{1}H\}$ NMR spectrum ($CDCl_3$, 100 MHz, 298 K) of 5,11,17,23-tetrabromo-25,26,27,28-tetrapropoxy-calix[4]arene (**CX3**).

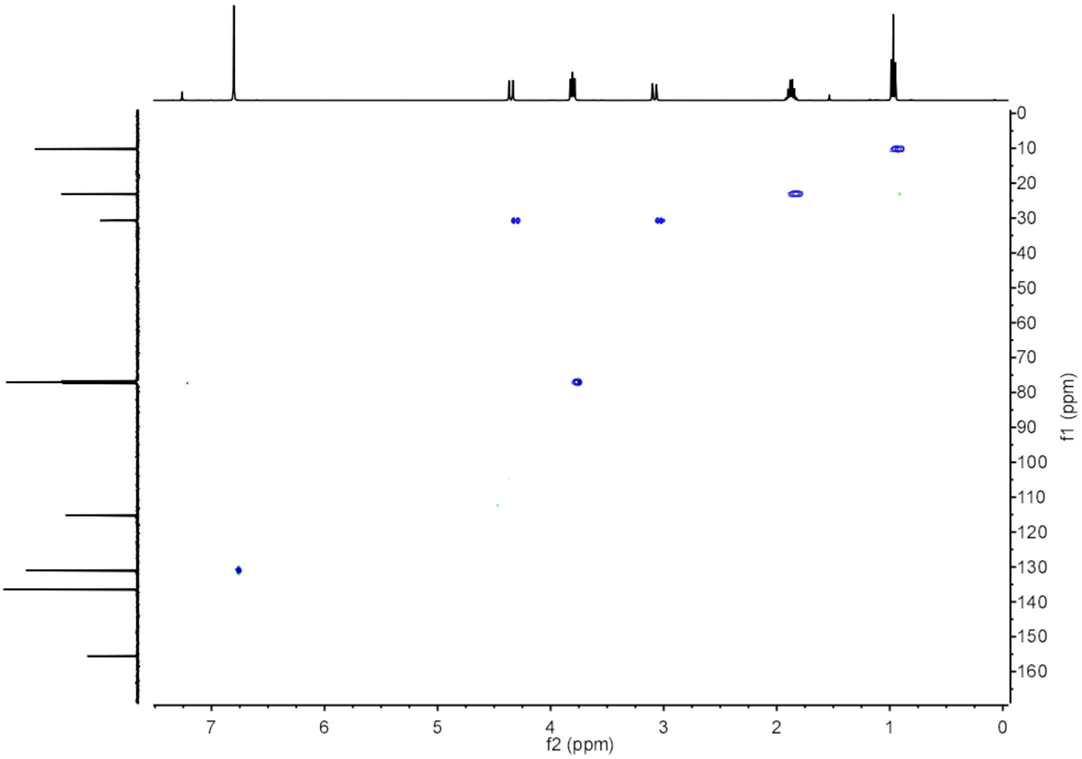

Figure S12. ^{1}H-^{13}C HSQC (400 MHz, $CDCl_3$, 297 K) spectrum of 5,11,17,23-tetrabromo-25,26,27,28-tetrapropoxy-calix[4]arene (**CX3**).

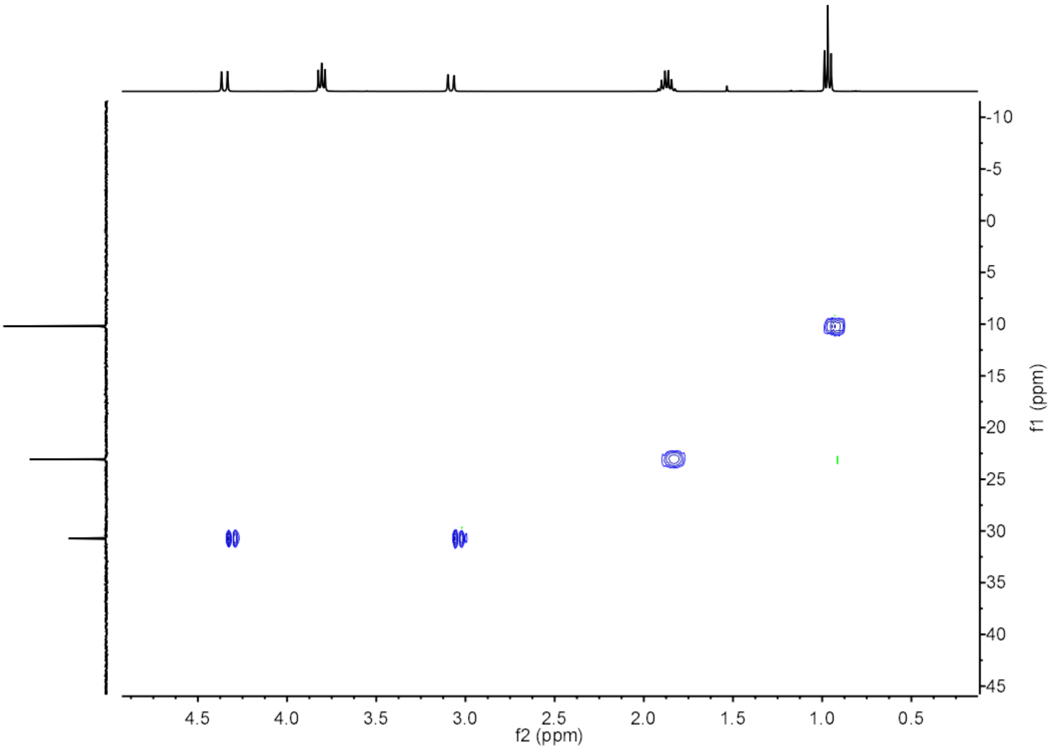

Figure S13. Aliphatic region of ^{1}H-^{13}C HSQC (400 MHz, $CDCl_3$, 297 K) spectrum of 5,11,17,23-tetrabromo-25,26,27,28-tetrapropoxy-calix[4]arene (**CX3**).

4 Infrared spectroscopy

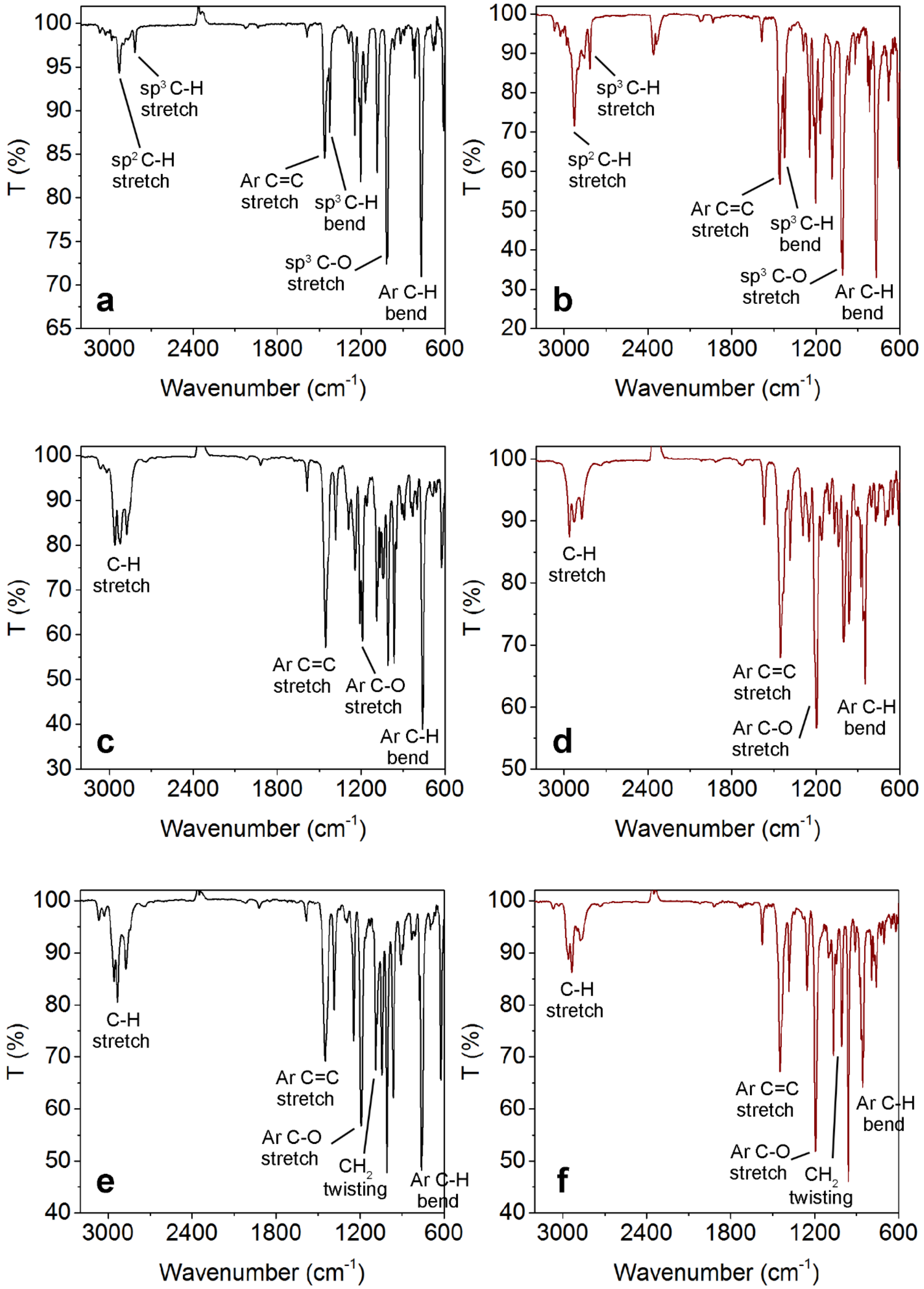

Figure S14. Infrared spectra of compounds **I** (a), **CX1** (b), **III** (c), **CX3** (d), **II** (e), **CX2** (f).

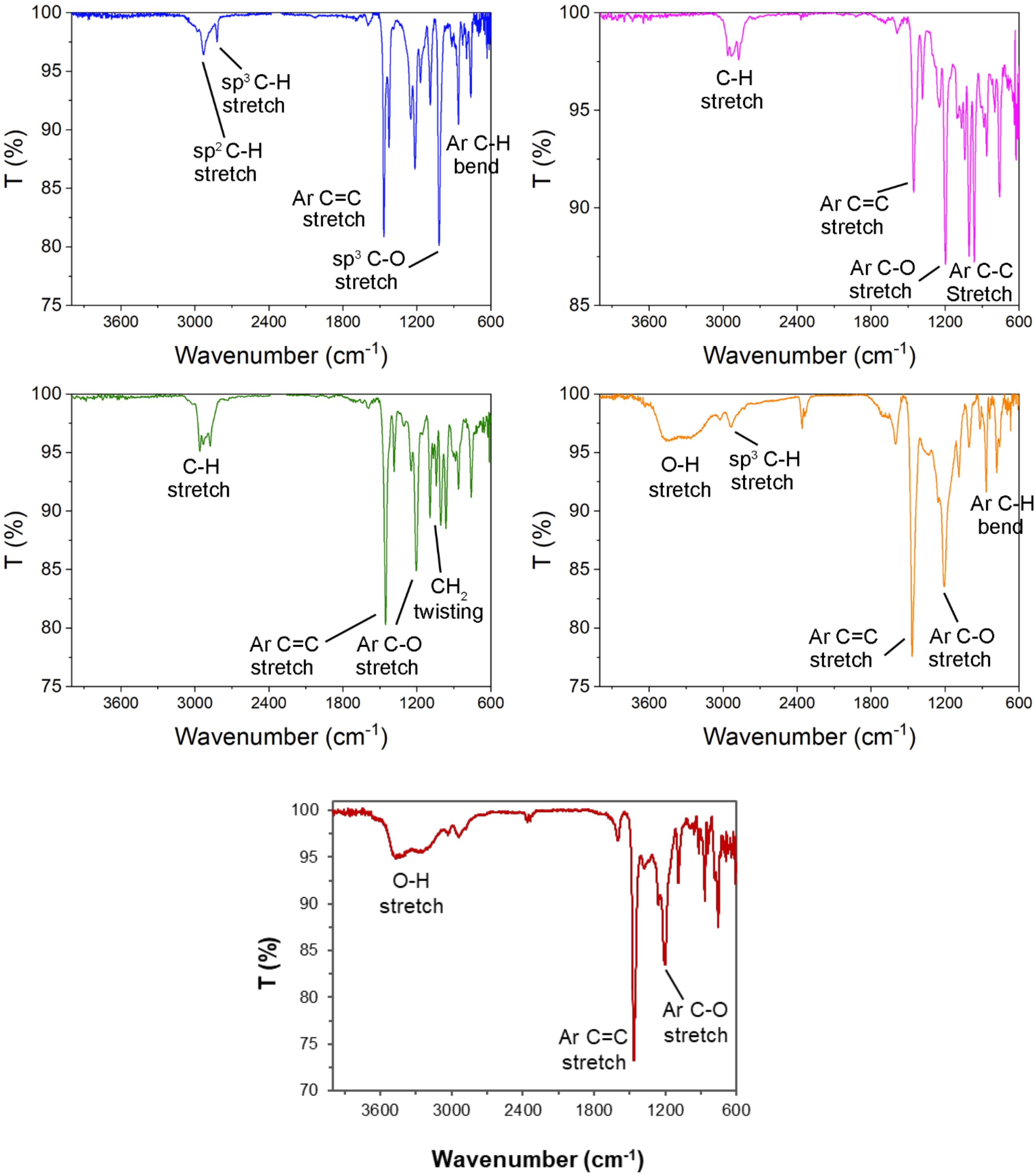

Figure S15. Infrared spectra of **CXF1-OMe** (blue), **CXF3-OPr** (pink), **CXF2-OPr** (green), **CXF1-OH** (orange) and **CXF2-OH** (red).

.

5 Powder X-ray diffraction (PXRD)

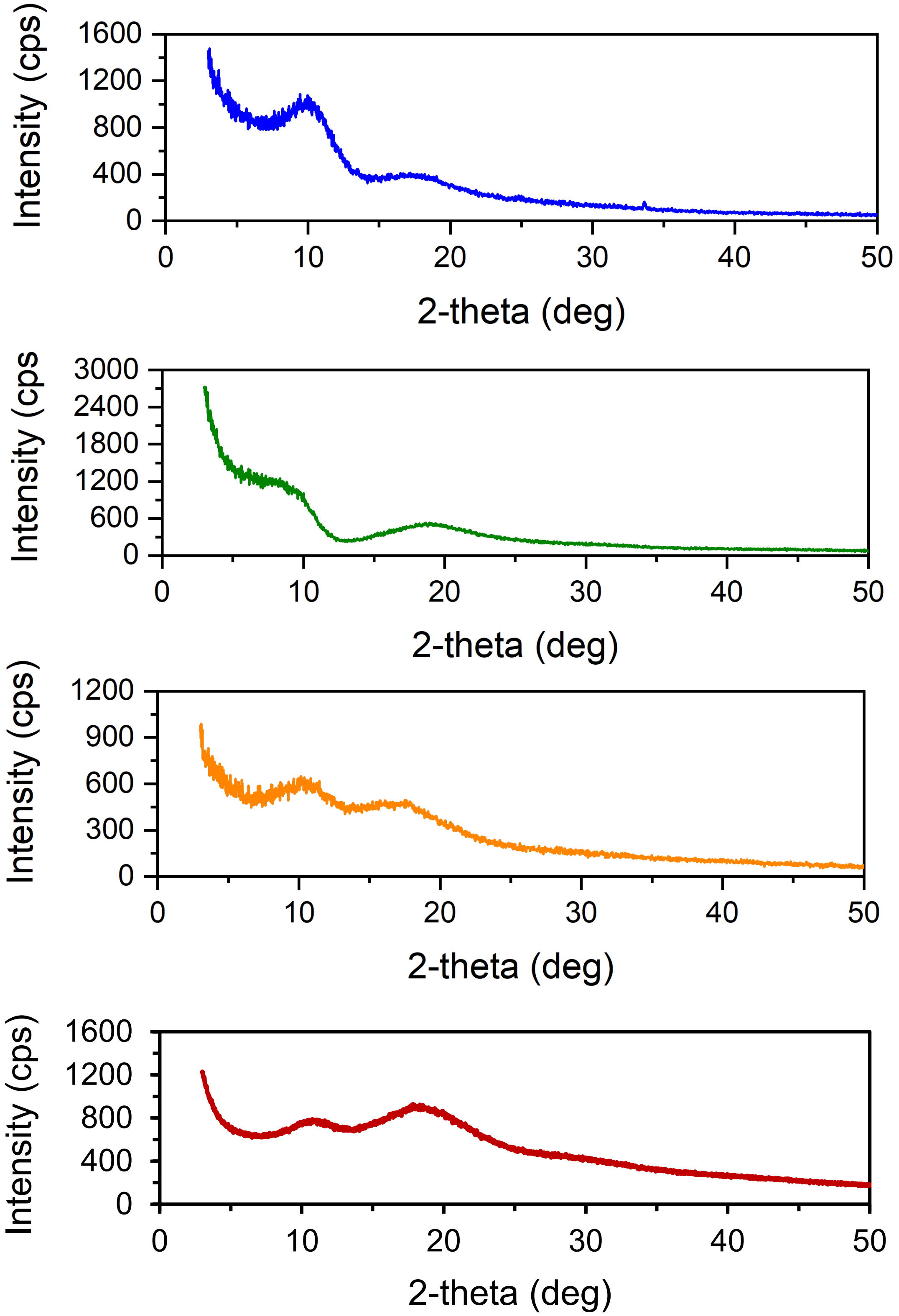

Figure S16. PXRD patterns of **CXF1-OMe** (blue), **CXF2-OPr** (green), **CXF1-OH** (orange) and **CXF2-OH** (red).

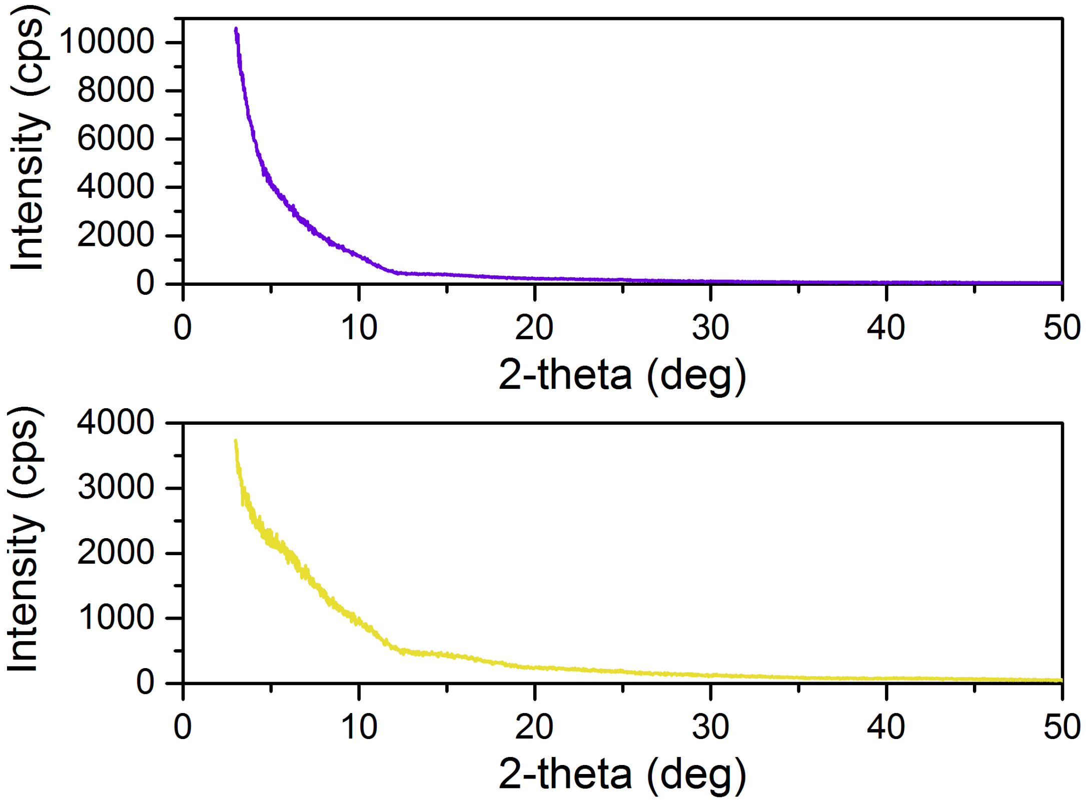

Figure S17. PXRD patterns of **co-CXF3-OPr** (purple) and **co-CXF3-OH** (yellow).

6 Thermal characterization

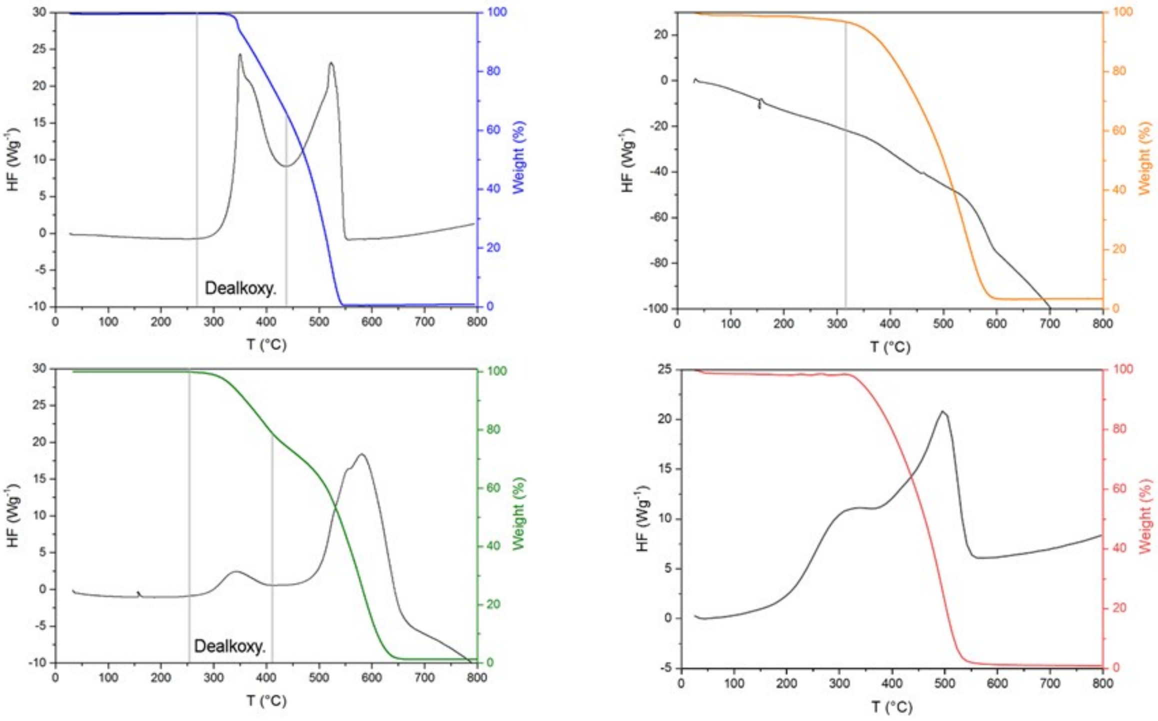

Figure S18. Differential scanning calorimetry (black trace) and thermogravimetric analyses (colored trace) carried out for **CXF1-OMe** (blue), **CXF2-OPr** (green), **CXF1-OH** (orange) and **CXF2-OH** (red) in a flow of air (50 mL/min) at a rate of 10 °C/min.

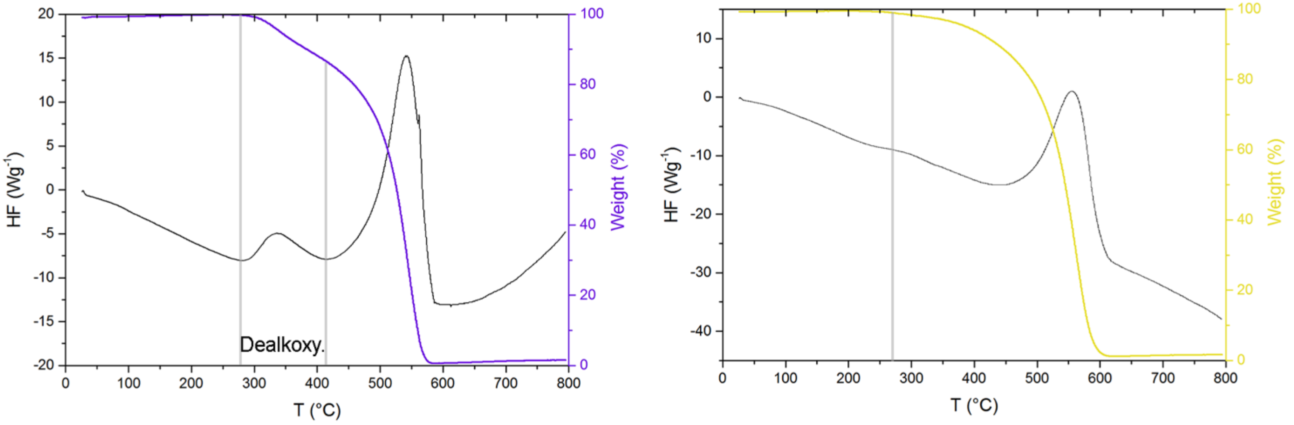

Figure S19. Differential scanning calorimetry (black trace) and thermogravimetric analyses (colored trace) carried out for **co-CXF3-OPr** (purple) and **co-CXF3-OH** (yellow) in a flow of air (50 mL/min) at a rate of 10 °C/min.

7 Solid State NMR

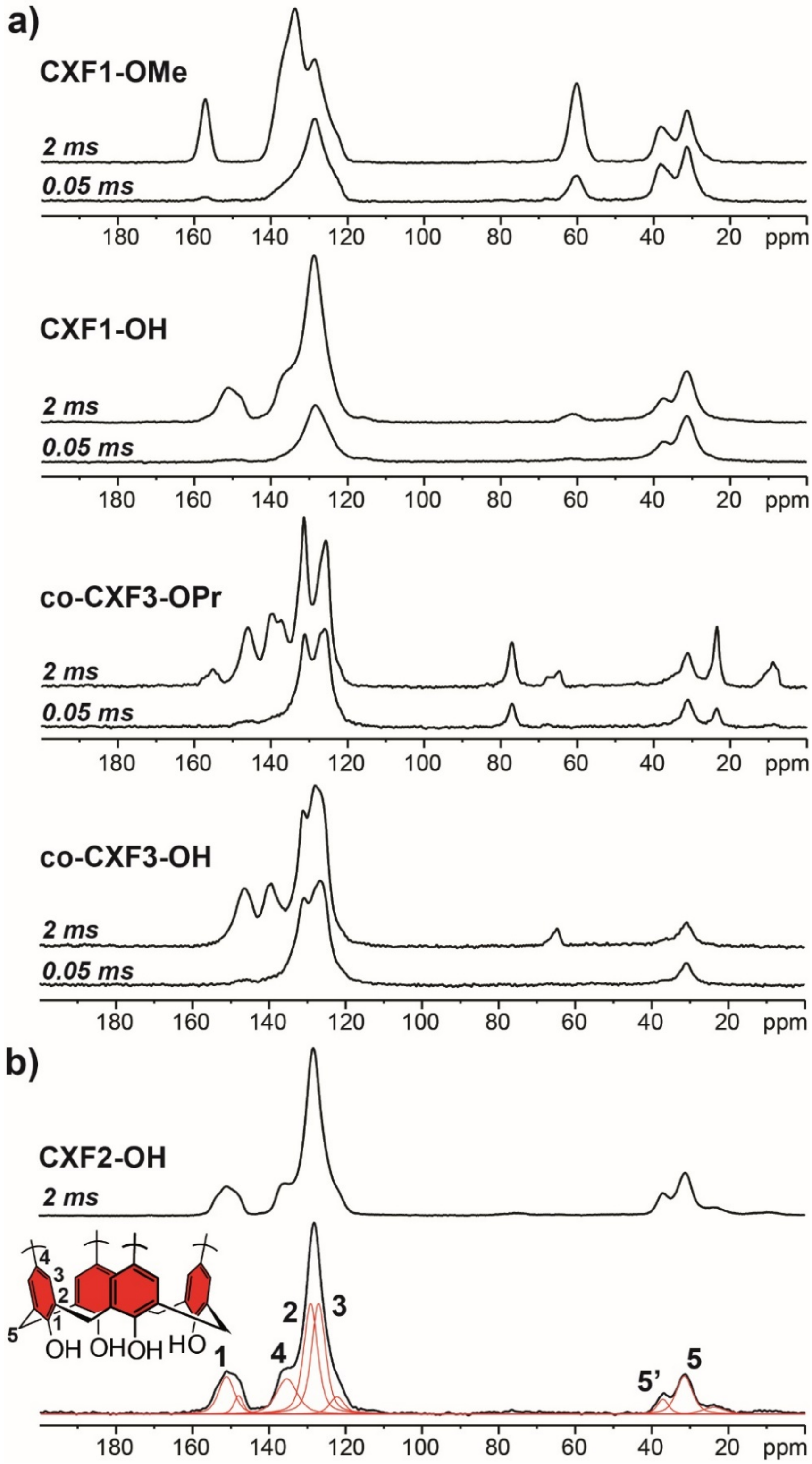

Figure S20. a) $^{13}C\{^{1}H\}$ CP MAS spectra of **CXF1-OMe**, **CXF1-OH**, **co-CXF3-OPr** and **co-CXF3-OH** performed at a spinning speed of 12.5 kHz and contact times of 2 ms and 0.05 ms. b) $^{13}C\{^{1}H\}$ CP MAS NMR spectrum of **CXF2-OH** performed at a spinning speed of 12.5 kHz and contact times of 2 ms and $^{13}C\{^{1}H\}$ MAS NMR spectrum of **CXF2-OH** with deconvoluted peaks (a recycle delay of 100 s was applied).

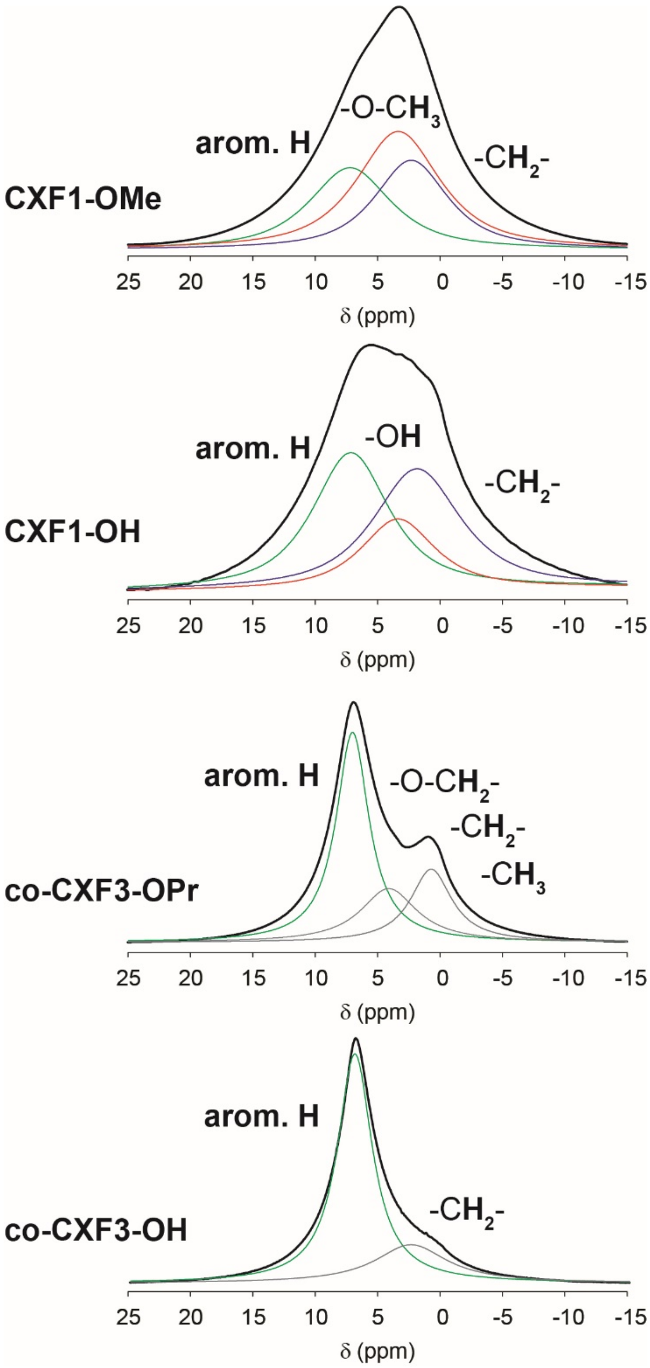

Figure S21. ^{1}H MAS spectra of **CXF1-OMe**, **CXF1-OH**, **co-CXF3-OPr** and **co-CXF3-OH** performed at a spinning speed of 12.5 kHz and recycle delay of 20 s.

Table S1. ^{13}C chemical shifts of **CXF1-OMe**, **CXF1-OH** and **CXF2-OH** from the simulation of quantitative ^{13}C{^{1}H} SPE MAS spectra collected with a recycle delay of 100 s at 293 K and 7.04 T.

	Assignment	**δ (ppm) ^{13}C{^{1}H} SPE MAS**
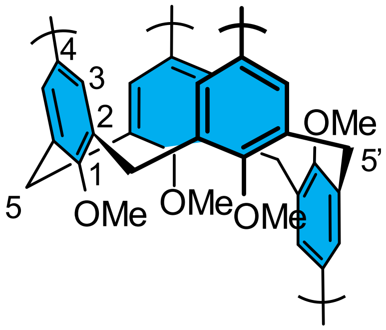	**C_1**	157.2
	C_2	133.9
	C_3	128.2
	C_4	137.3
	C_5	31.2
	$C_{5'}$	37.9
	-OMe	60.2
	Assignment	**δ (ppm) ^{13}C{^{1}H} SPE MAS**
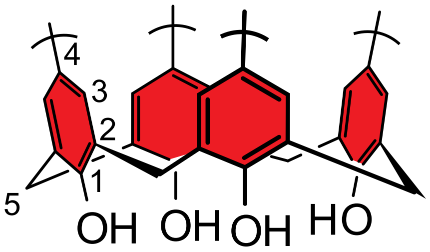	**CXF1-OH**	
	C_1	151.3
	C_2	130.0
	C_3	127.6
	C_4	135.6
	C_5	31.0
	$C_{5'}$	37.5
	CXF2-OH	
	C_1	151.3
	C_2	129.3
	C_3	127.3
	C_4	135.5
	C_5	31.5
	$C_{5'}$	37.1

Table S2. ^{13}C chemical shifts of **co-CXF3-OPr** from the simulation of quantitative ^{13}C{^{1}H} SPE MAS spectrum collected with a recycle delay of 100 s at 293 K and 7.04 T.

	Assignment	**δ (ppm) ^{13}C{^{1}H} SPE MAS**	**Amount %**
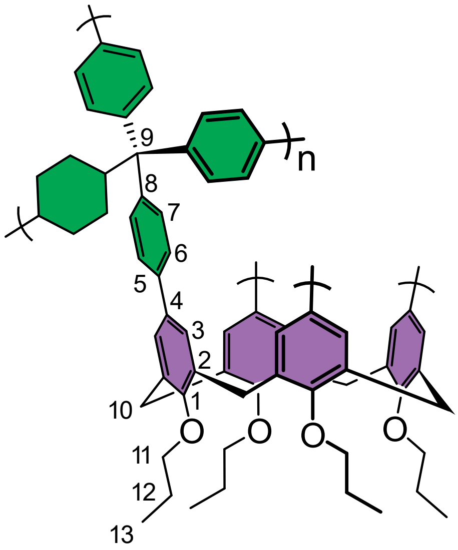	C$_1$	155.9	3.2
	C$_2$	133.3	6.3
	C$_3$	127.8	6.5
	C$_4$	137.2	3.2
	C$_5$	146.3	11.1
	C$_6$	125.7	20.9
	C$_7$	131.4	21.5
	C$_8$	139.9	11.5
	C$_9$	64.7	2.7
	C$_{10}$	31.20	3.4
	C$_{11}$	77.1	3.2
	C$_{12}$	23.6	3.1
	C$_{13}$	8.9	3.3

Table S3. ^{13}C chemical shifts of **co-CXF3-OH** from the simulation of quantitative $^{13}C\{^1H\}$ SPE MAS spectrum collected with a recycle delay of 100 s at 293 K and 7.04 T.

	Assignment	**δ (ppm)** **$^{13}C\{^1H\}$ SPE MAS**	**Amount** **%**
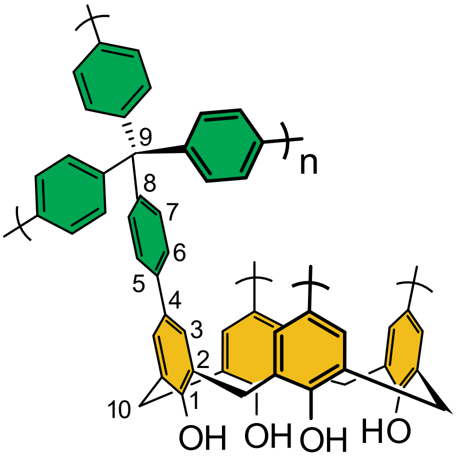	C_1	148.6	3.0
	C_2	132.9	6.1
	C_3	128.0	5.9
	C_4	137.3	3.0
	C_5	146.0	12.7
	C_6	126.3	25.6
	C_7	130.8	25.4
	C_8	140.2	12.5
	C_9	64.5	3.1
	C_{10}	31.5	3.0

8 Scanning electron microscopy

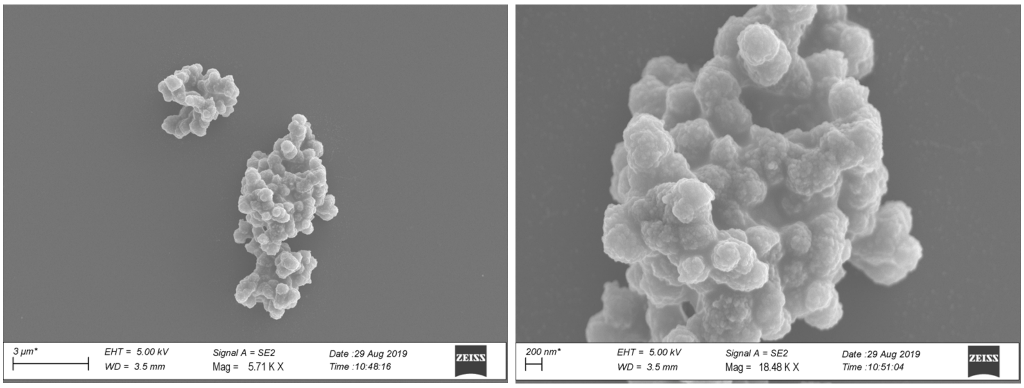

Figure S22. Scanning electron microscope images of **CXF1-OMe** drop-casted on a silicon substrate.

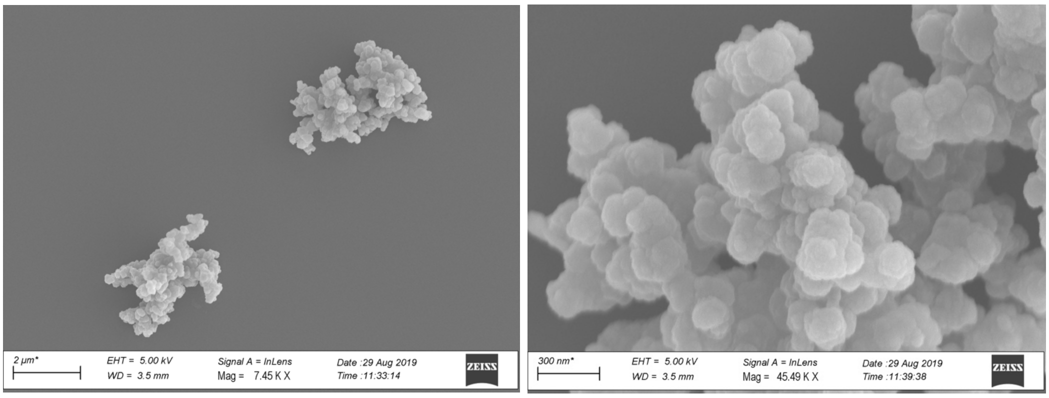

Figure S23. Scanning electron microscope images of **CXF1-OH** drop-casted on a silicon substrate.

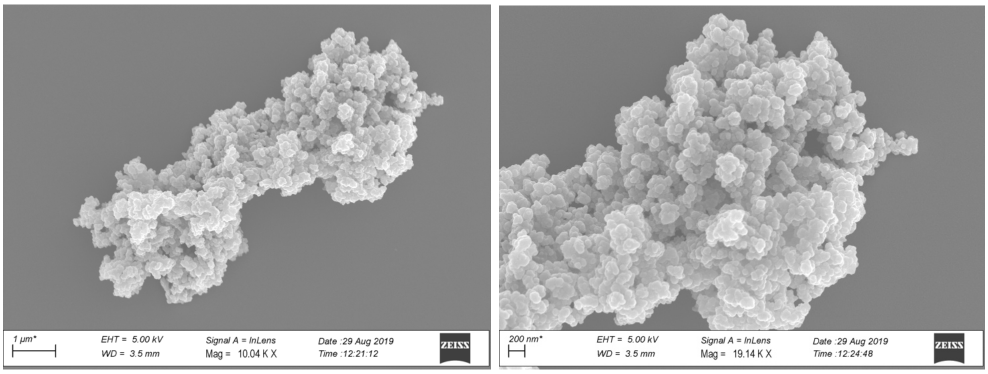

Figure S24. Scanning electron microscope images of **co-CXF3-OPr** drop-casted on a silicon substrate.

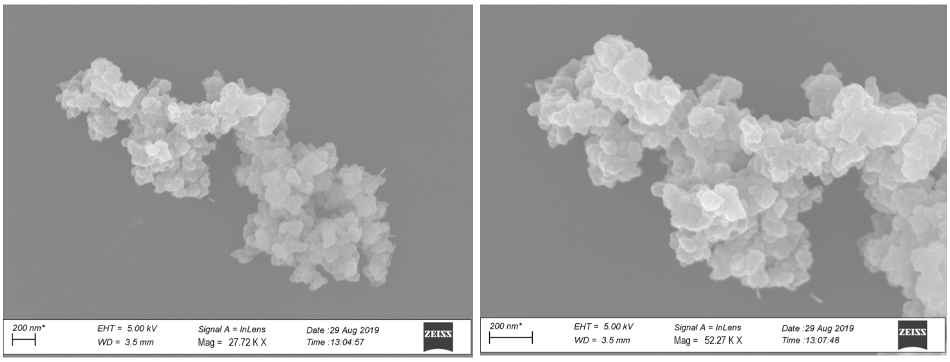

Figure S25. Scanning electron microscope images of **co-CXF3-OH** drop-casted on a silicon substrate.

9 Elemental Analyses

Table S4. Calculated versus experimental CHN percentage values for CXFs.

	C		H		N	
	Calc.	Exp.	Calc.	Exp.	Calc.	Exp.
CXF1-OMe	80.65%	83.32%	5.92%	5.99%	0%	0.44%
co-CXF3-OPr[a]	90.68%	87.83%	5.87%	5.57%	0%	0.14%

[a] calculated values based on initial CX3/tetraphenylmethane ratio of 1:4.

10 Helium Pycnometry

Table S5. Skeletal density values for **CXFs** as derived from He pycnometry.

	Skeletal density **(g/cm^3)**
CXF1-OMe	1.255 (± 0.001)
CXF1-OH	1.366 (± 0.001)
co-CXF3-OPr	1.293 (± 0.006)
co-CXF3-OH	1.352 (± 0.002)

11 Gas adsorption measurements for CXFs

11.1 N_2 adsorption

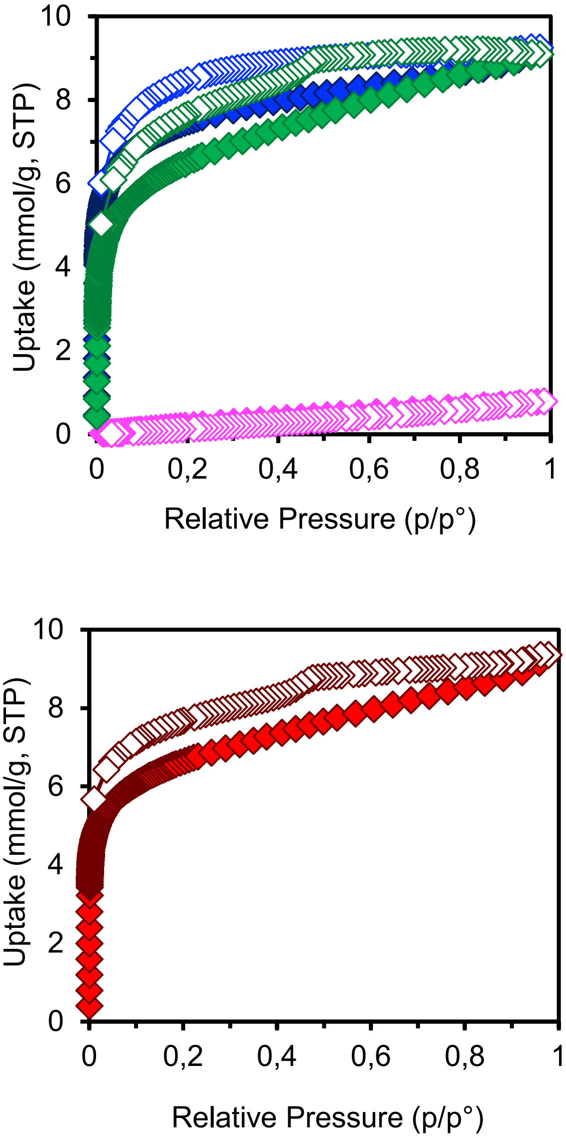

Figure S26. N_2 adsorption isotherms collected at 77 K and up to 1 bar: (top) **CXF1-OMe** (blue), **CXF2-OPr** (green) and **CXF3-OPr** (pink); (down) **CXF2-OH** (red). Empty symbols define the desorption branch.

Table S6. Textural parameters of **CXFs** as derived from N_2 adsorption isotherms at 77 K.

	S_{Langmuir}[a] (m^2 g^{-1})	S_{BET}[a] (m^2 g^{-1})	V_{total}[b] (cm^3 g^{-1})
CXF1-OMe	687	626	0.293
CXF2-OPr	638	562	0.291
CXF1-OH	610	540	0.324
CXF2-OH	621	546	0.301

[a] calculated using adsorption data in p/p° range from 0.015 to 0.1

[b] calculated using Non-Local Density Functional Theory and Carbon Slit Pores model

12 Hyperpolarized ^{129}Xe NMR

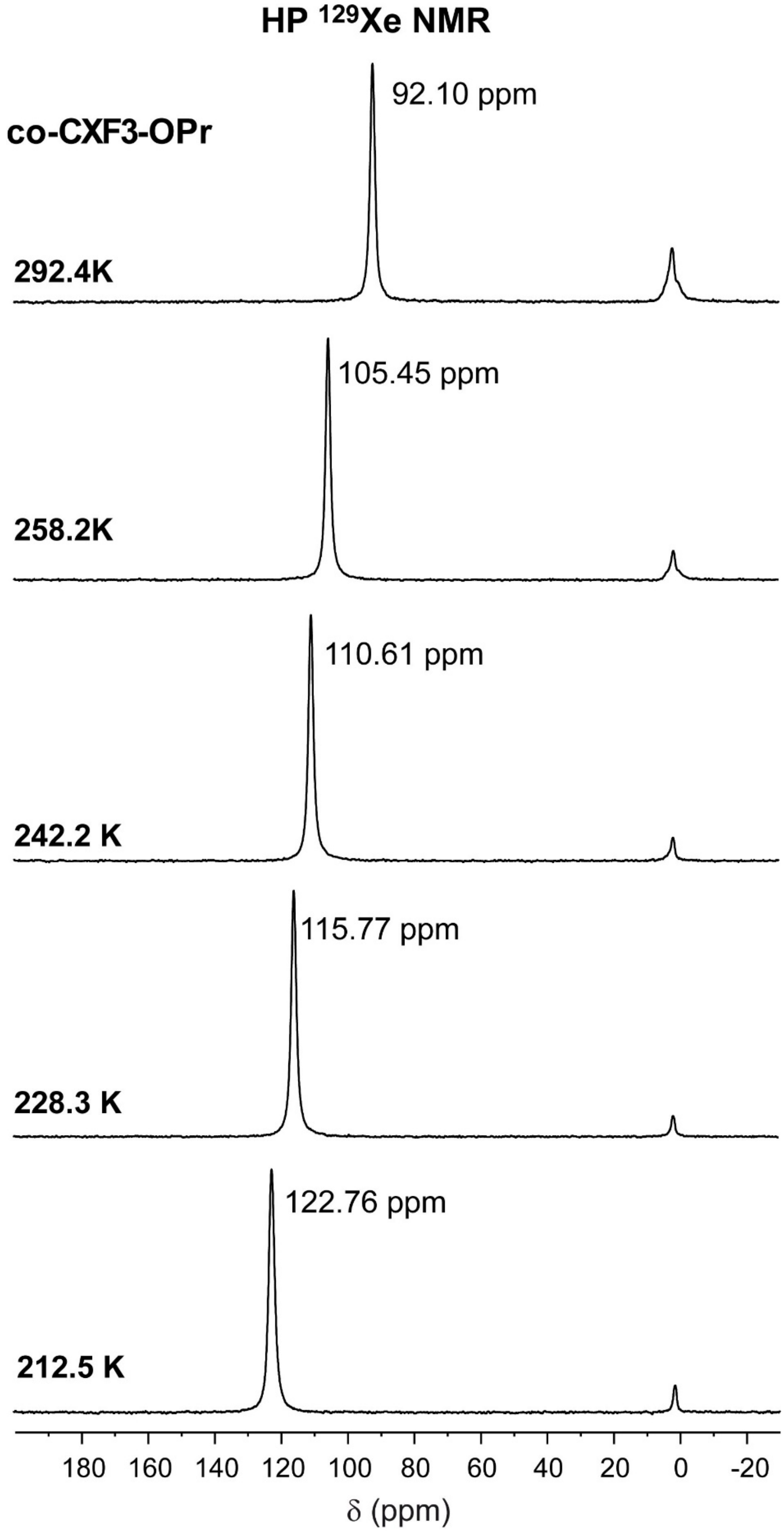

Figure S27. Variable temperature HP ^{129}Xe NMR spectra of **co-CXF3-OPr**.

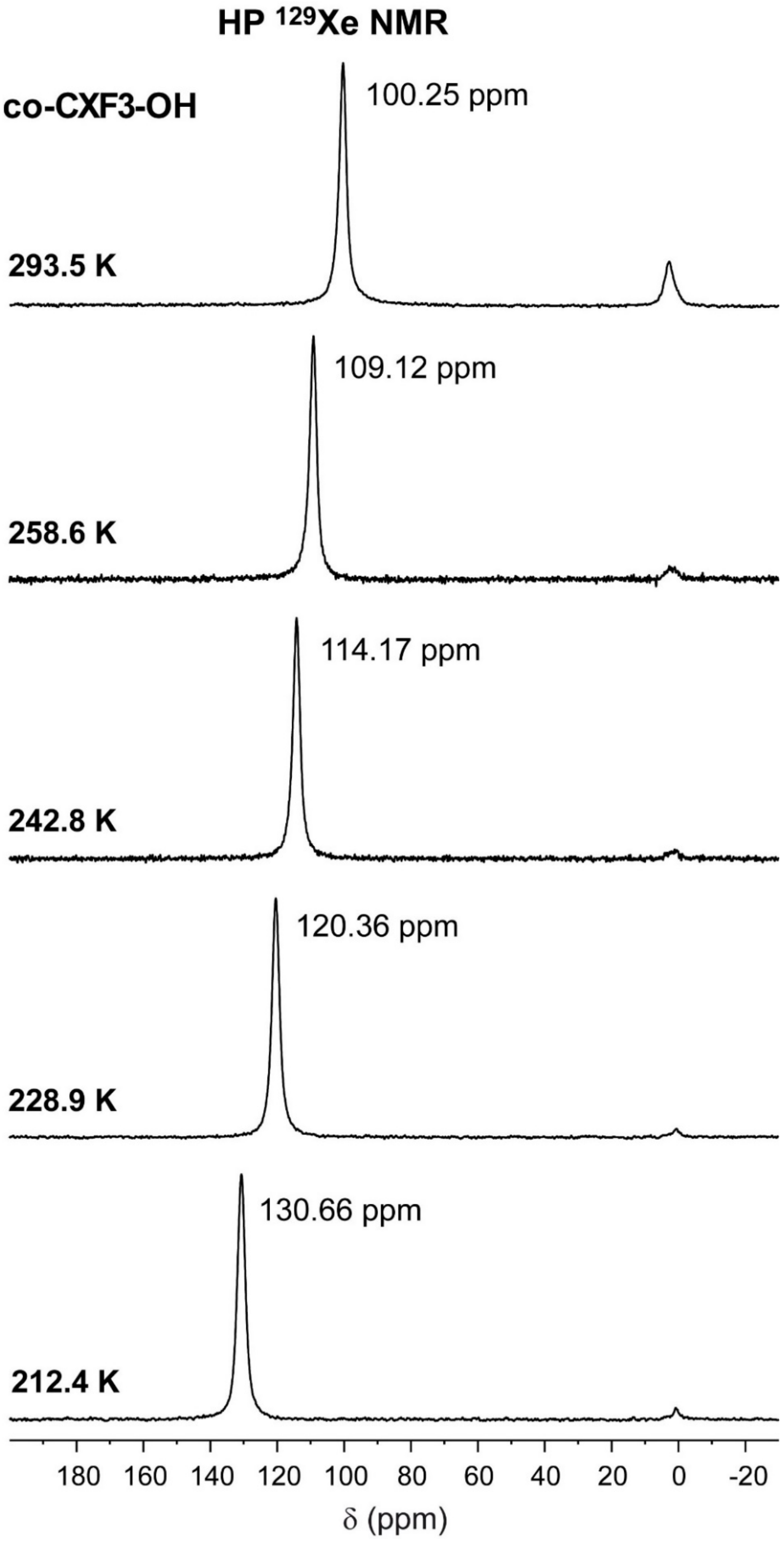

Figure S28. Variable temperature HP ^{129}Xe NMR spectra of **co-CXF3-OH**.

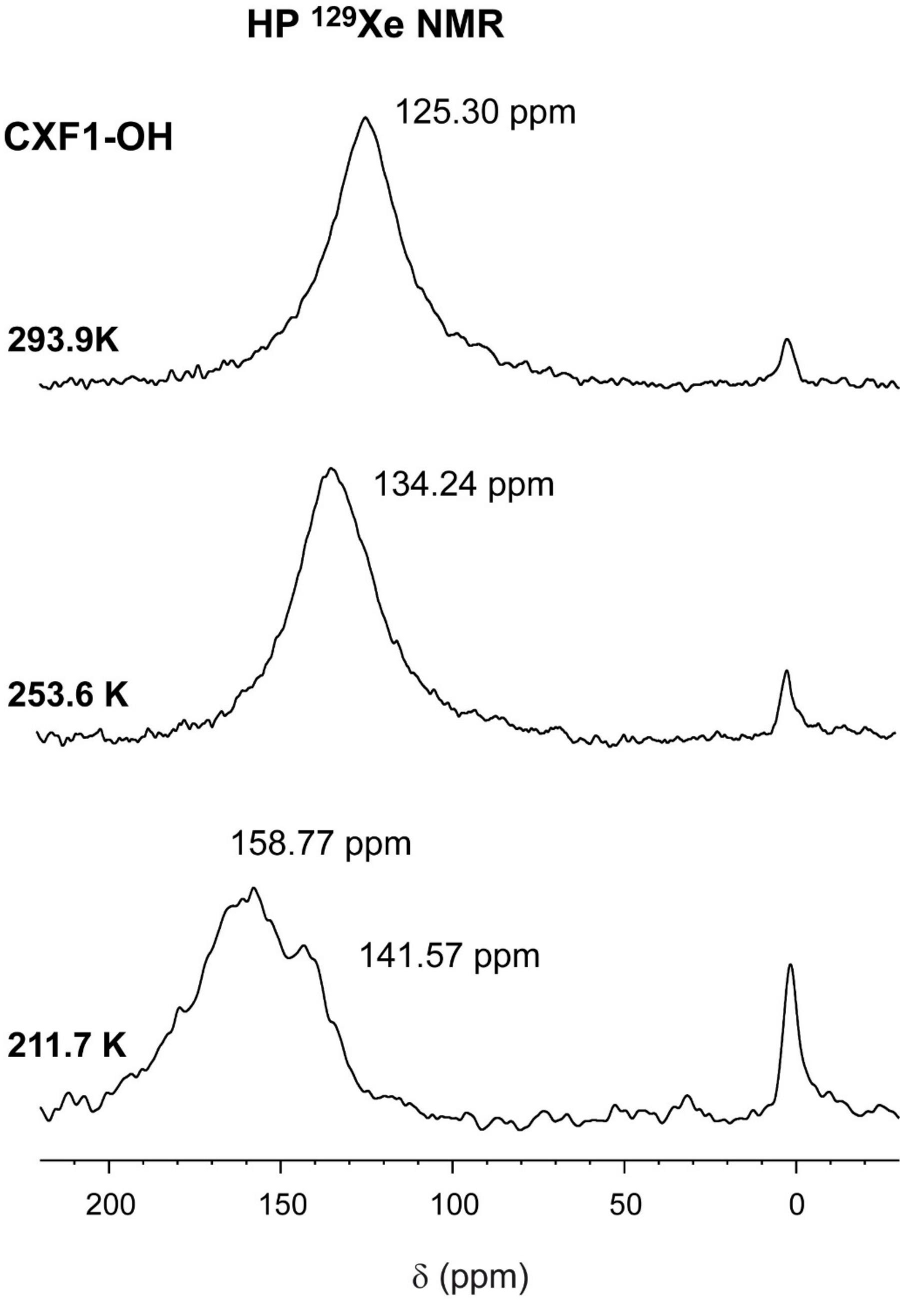

Figure S29. Variable temperature HP ^{129}Xe NMR spectra of **CXF1-OH**.

13 CO_2 adsorption (CXF1-OMe and CXF1-OH)

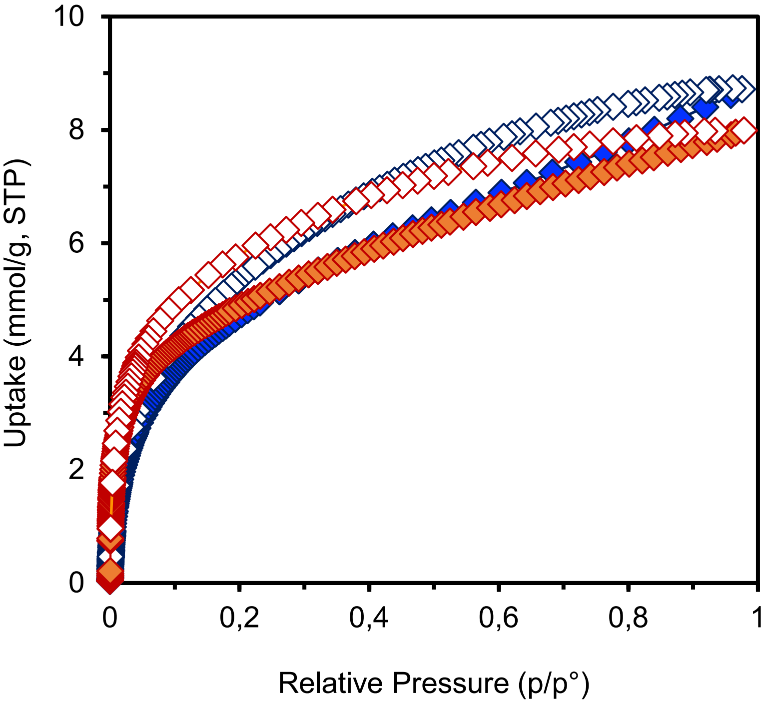

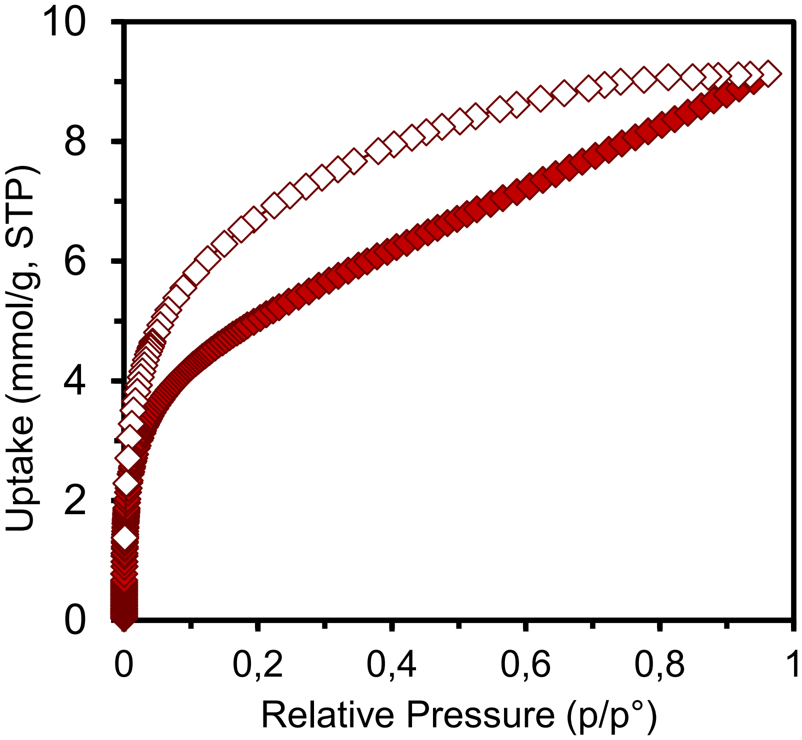

Figure S30. CO_2 adsorption isotherm collected at 195 K and up to 1 bar. (Above) **CXF1-OMe** (blue) and **CXF1-OH** (orange). (Below) **CXF2-OH** (red). Empty symbols define the desorption branch.

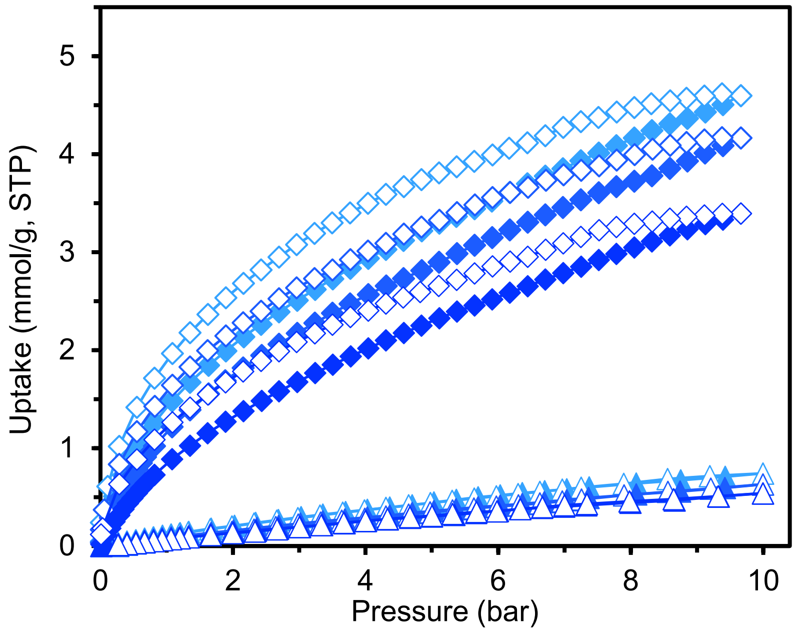

Figure S31. CO_2 (diamonds) and N_2 (triangles) adsorption isotherms of **CXF1-OMe** collected at 273 K (light blue), 283 K (blue) and 298 K (dark blue) up to 10 bar. Empty symbols define the desorption branch.

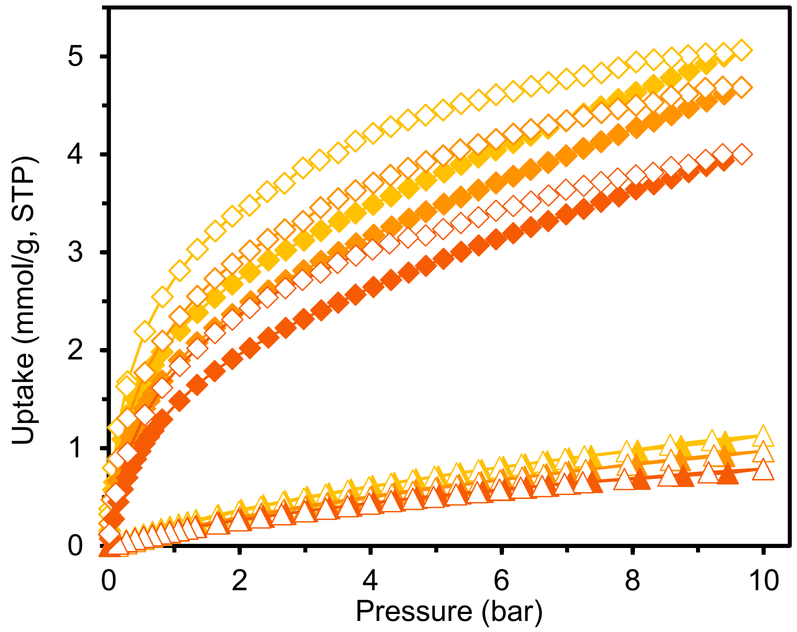

Figure S32. CO_2 (diamonds) and N_2 (triangles) adsorption isotherms of **CXF1-OH** collected at 273 K (light orange), 283 K (orange) and 298 K (dark orange) up to 10 bar. Empty symbols define the desorption branch.

$Q_{st}(CO_2)$ was derived from CO_2 adsorption isotherms collected at 273 K, 283 K and 298 K up to 10 bar using the van't Hoff equation:

$$Q_{st} = RT^2\left(\frac{\partial \ln p}{\partial T}\right) \qquad (eq.\ S1)$$

First, the three isotherms were fitted adopting a dual-site Langmuir model:

$$\boldsymbol{q} = \boldsymbol{q}_A + \boldsymbol{q}_B = \frac{q_{sat,A} b_A p}{1+b_A p} + \frac{q_{sat,B} b_B p}{1+b_B p} \qquad (eq.\ S2)$$

Where **q** is the adsorbed quantity at the pressure p, $\mathbf{q}_A$ and $\mathbf{q}_B$ are the quantities adsorbed by sites A and B, respectively, at pressure p, $q_{sat,A}$ and $q_{sat,B}$ are the maximum adsorbed quantities by site A and B, respectively, at infinite pressure and b_A and b_B are defined as

$$b_A = b_{0,A} exp(E_A/RT) \qquad (eq.\ S3)$$

$$b_B = b_{0,B} exp(E_B/RT) \qquad (eq.\ S4)$$

It follows that we can define an energy E_A for adsorption on site A and an energy E_B for adsorption on site B. Calculations were run using Mathlab software: the calculated fitting parameters are reported in Table S7, while Figure S33 shows the fitted curve over the experimental isotherms. From the dual-site Langmuir equation, we can derive an analytical expression for the pressure:

$$p = \frac{-\beta + \sqrt{\beta^2 + 4\alpha \boldsymbol{q}}}{2\alpha} \qquad (eq.\ S5)$$

and calculate Q_{st} *via* the van't Hoff equation (*eq. S1*). For **CXF1-OMe** a Q_{st} value of 26 kJ mol^{-1} was calculated.

Table S7. Fitting parameters obtained for carbon dioxide adsorption for **CXF1-OMe** and **CXF1-OH** using a dual-site Langmuir model.

	$Q_{sat,A}$ (mmol/g)	$Q_{sat,B}$ (mmol/g)	$b_{0,A}$ (bar^{-1})	$b_{0,B}$ (bar^{-1})	E_A (kJ/mol)	E_B (kJ/mol)
CXF1-OMe	1	6.3155	$8.93 \cdot 10^{-6}$	$3.85 \cdot 10^{-5}$	28.6211	18.2228
CXF1-OH	1.5208	6.3734	$4.31 \cdot 10^{-6}$	$5.16 \cdot 10^{-5}$	32.5985	17.6361

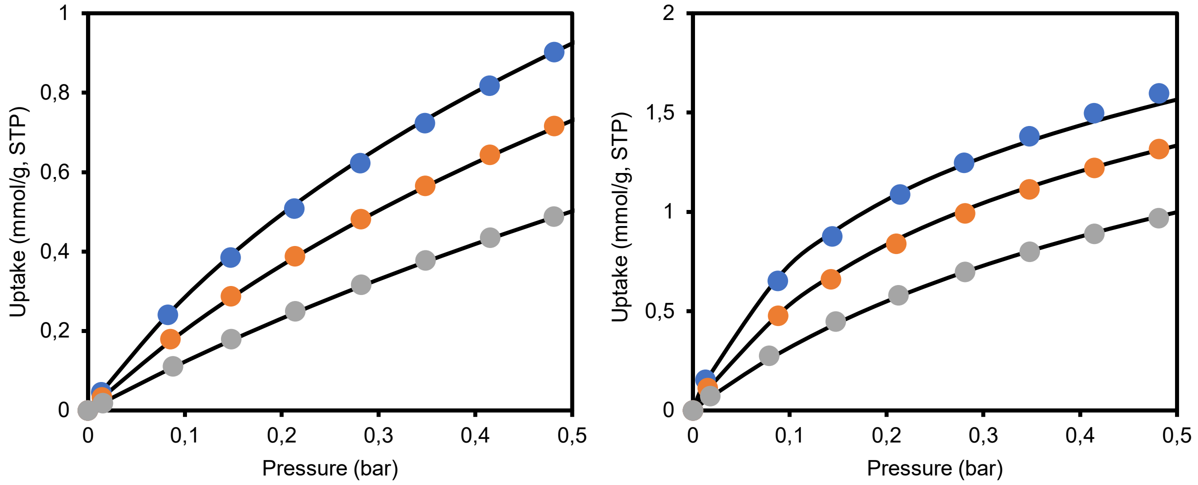

Figure S33. Fitting of experimental isotherms for **CXF1-OMe** (left) and **CXF1-OH** (right). CO_2 isotherms at 273 K (blue), 283 K (orange), 298 K (grey) and fitting (solid black trace) are reported.

Table S8. CO_2 adsorption capacities at 10 and 1 bar reported as mmol/g and wt % and CO_2/N_2 selectivities for **CXFs**.

	T (K)	P (bar)	$Q_{10bar}(CO_2)$ (mmol/g)	(Q_{10bar}) wt%	$Q_{1bar}(CO_2)$ (mmol/g)	(Q_{1bar}) wt%	Selectivity[c]
CXF1-OMe	195	1[a]	8.7	38.3	/	/	/
	273	10	4.6	20.2	1.5	6.6	68
	283	10	4.2	18.5	1.2	5.3	/
	298	10	3.4	15.0	0.9	4.0	/
CXF1-OH	195	1[a]	8.1	35.6	/	/	/
	273	10	5.1	22.4	2.2	9.7	98
	283	10	4.5	19.8	1.9	8.4	/
	298	10	3.9	17.2	1.5	6.6	/

[a] p/p° is reported

[b] From microcalorimetry.

c Value calculated applying the IAST theory to a 15:85 CO_2/N_2 mixture at 1 bar.

14 Adsorption coupled microcalorimetry (CXF1-OH)

The enthalpy variation related to CO_2 adsorption was measured *via* sorption-coupled microcalorimetry experiments.[6]

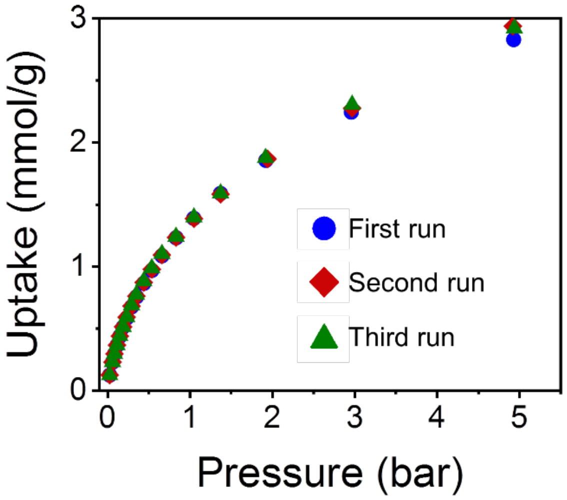

Figure S34. CO_2 adsorption isotherms of **CXF1-OH** collected at 293 K coupled with microcalorimetry. Sorption-coupled microcalorimetry measurements were performed three times at 293 K and the three different runs were averaged to reduce experimental errors.

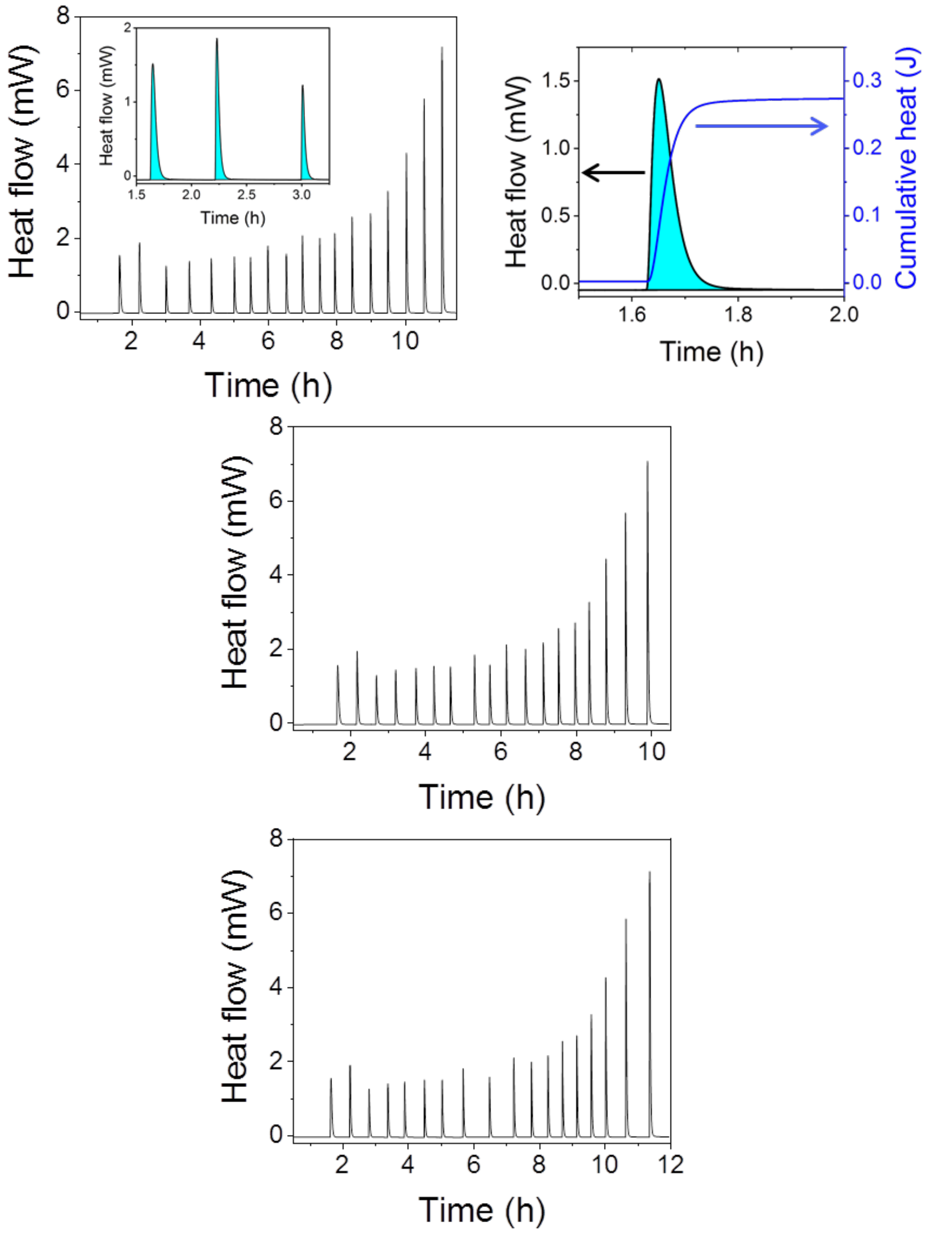

Figure S35. Top, left: heat flow measured during CO_2 adsorption for sample **CXF1-OH** using the ASAP 2050 and µDSC7 coupled system. Each peak represents a gas dose and therefore an adsorption point. Inset: enlargement of the DSC thermogram showing the first 3 peaks. Top, right: The DSC thermogram was integrated over time to calculate the integral heat released during the adsorption process. Middle, bottom: The measurements were repeated three times to assess reproducibility, second and third cycles are reported.

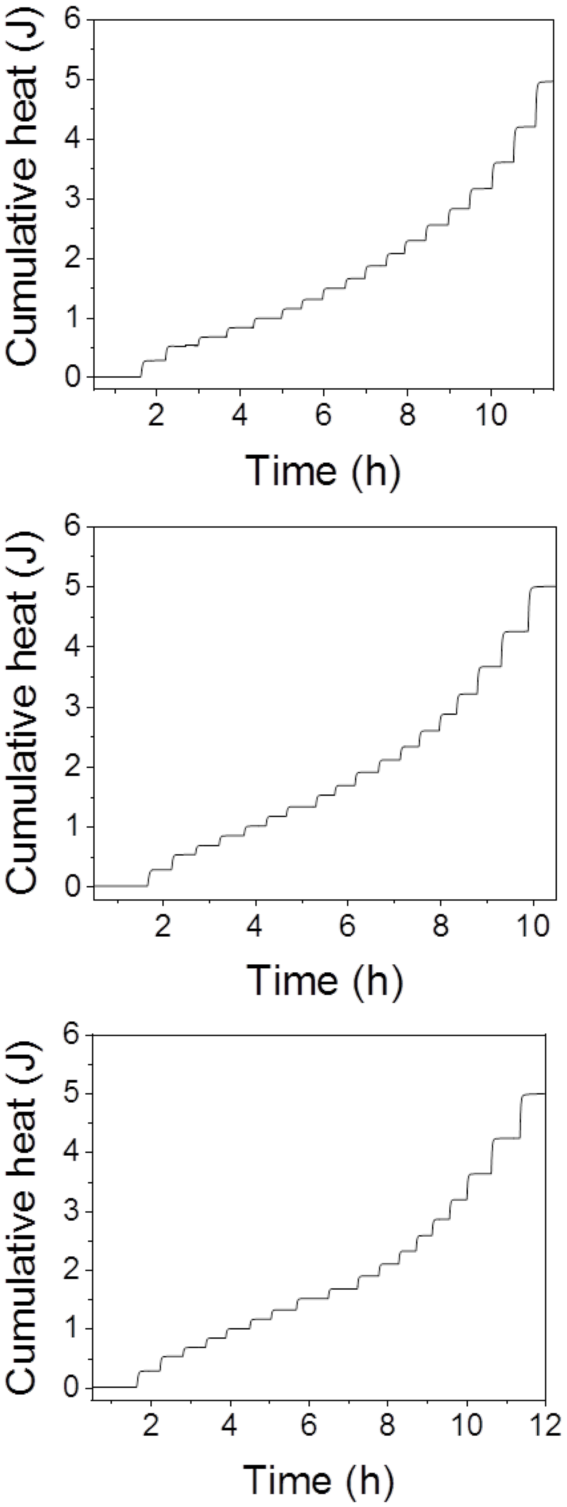

Figure S36. Integral heat released during the adsorption of CO_2 for sample **CXF1-OH**. First (top), second (middle) and third (bottom) runs are reported.

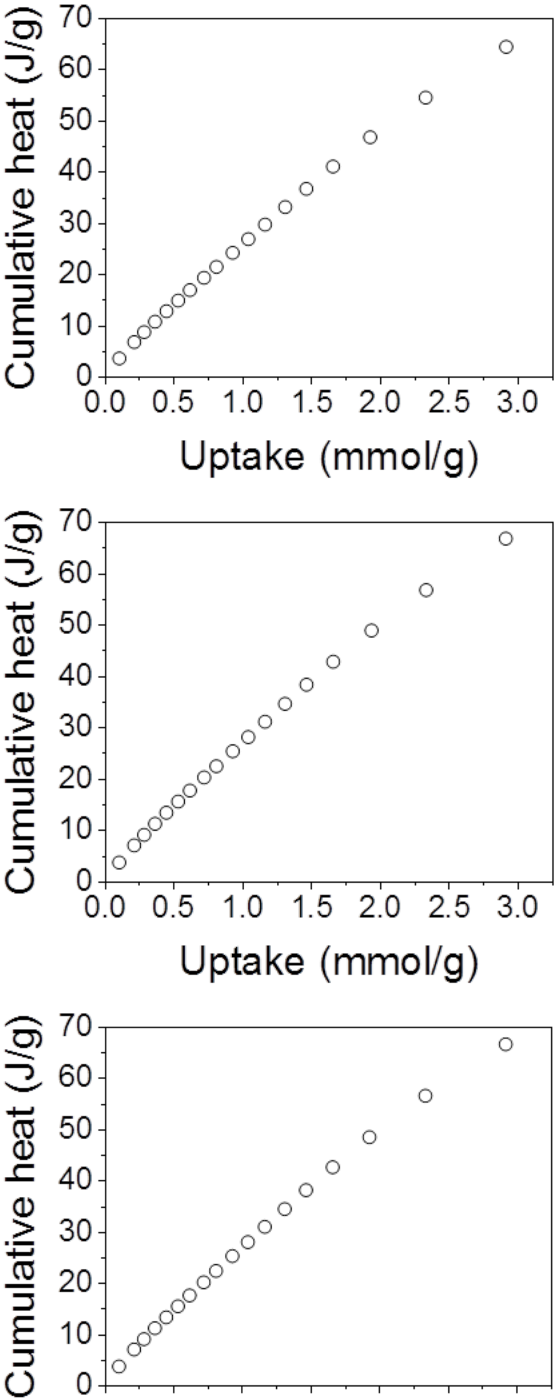

Figure S37. Normalized integral heat (J/g) versus uptake (mmol/g) for the first (top), second (middle) and third run (bottom) for sample **CXF1-OH**.

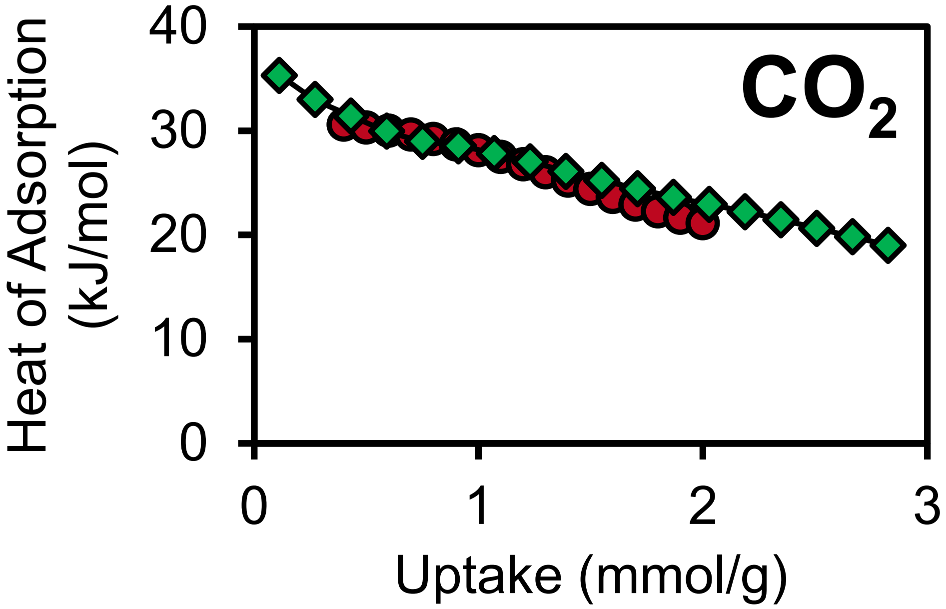

Figure S38. Isosteric heat of adsorption of CO_2 of **CXF1-OH** calculated from adsorption isotherms collected at different temperatures (273 K, 283 K and 298 K) using the van't Hoff equation (red circles) and directly measured with sorption-coupled microcalorimetry (green diamonds). Microcalorimetry provides accurate measurements of adsorption enthalpy especially at very low coverage while isosteric method may present serious inaccuracies in the same region, therefore, we took under consideration microcalorimetry data at low coverage.[7] Microcalorimetry measurements were repeated three times resulting in the following adsorption enthalpy values of 35.3, 35.0 and 35.4 kJ mol^{-1}.

15 CO_2/N_2 Selectivity (CXF1-OMe and CXF1-OH)

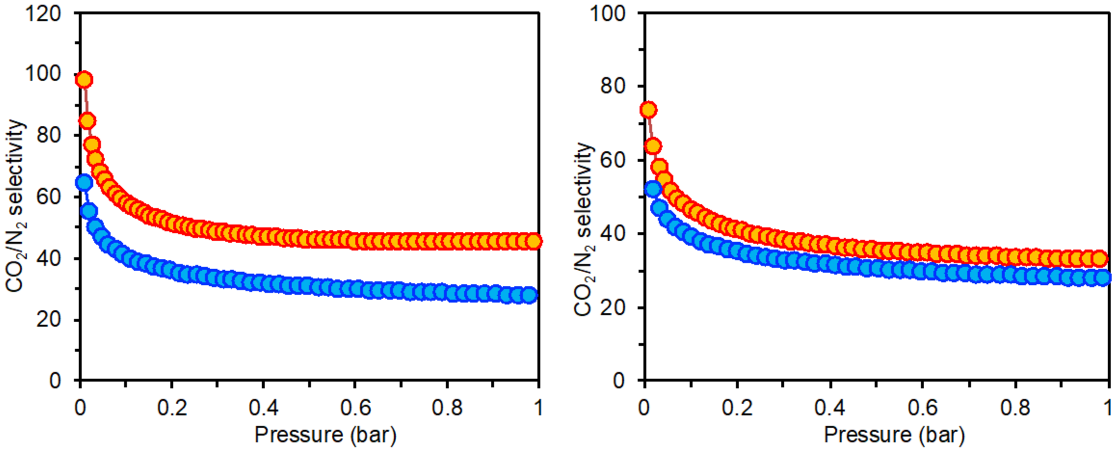

Figure S39. IAST selectivity for the adsorption of CO_2 over N_2 from a 15:85 mixture calculated at 273 K (left) and 298 K (right) for **CXF1-OMe** (blue) and **CXF1-OH** (orange).

16 Column breakthrough analysis (CXF1-OH)

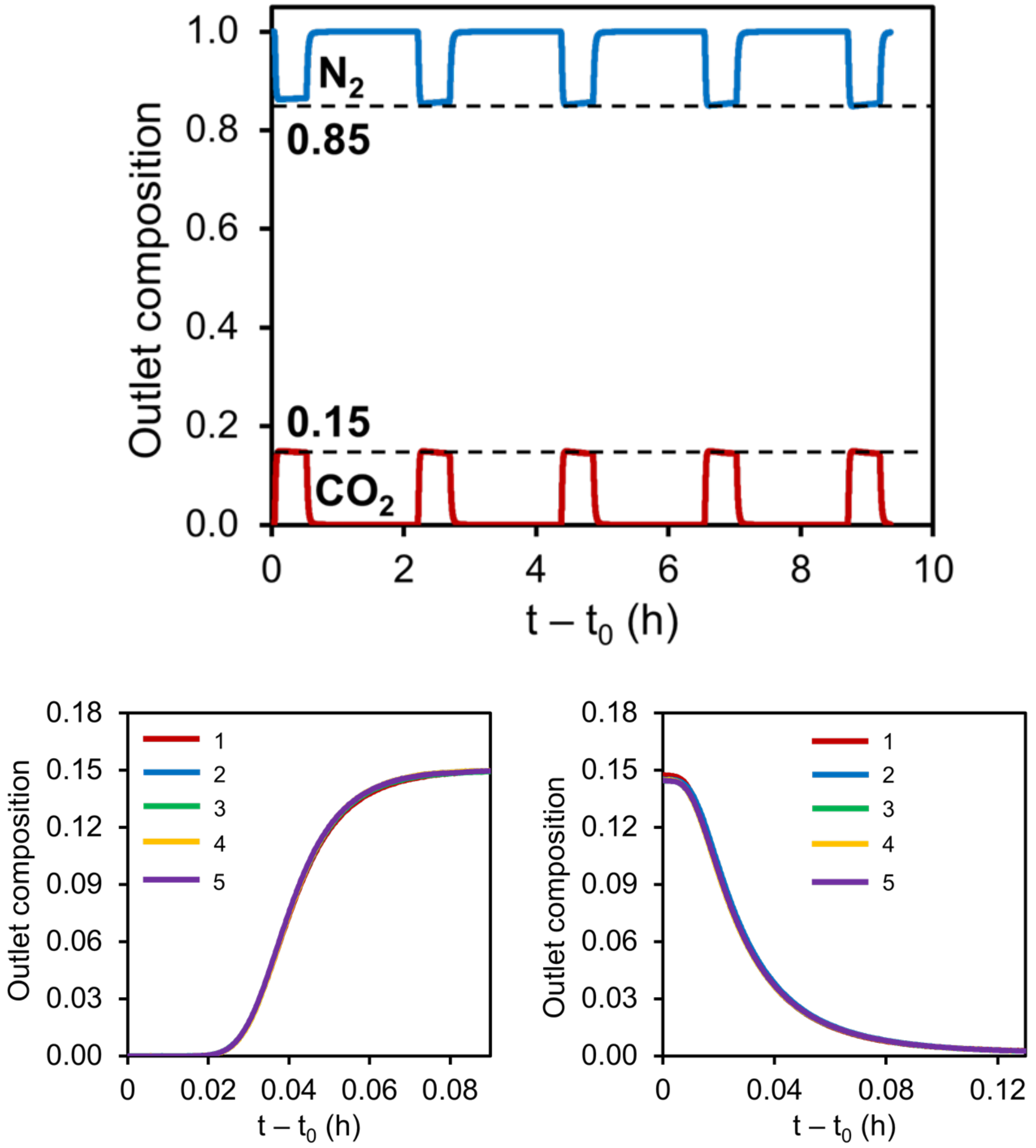

Figure S40. Multiple breakthrough cycles collected using a mixture of CO_2/N_2 (15/85) at 298 K on **CXF1-OH** sample. The sample was regenerated by flowing pure nitrogen at 20 sccm for 90 minutes at 298 K. Time was corrected taking into account the dead time and blank measurements. Bottom: breakthrough and regeneration curves for each cycle are overlayed showing complete recyclability at each cycle.

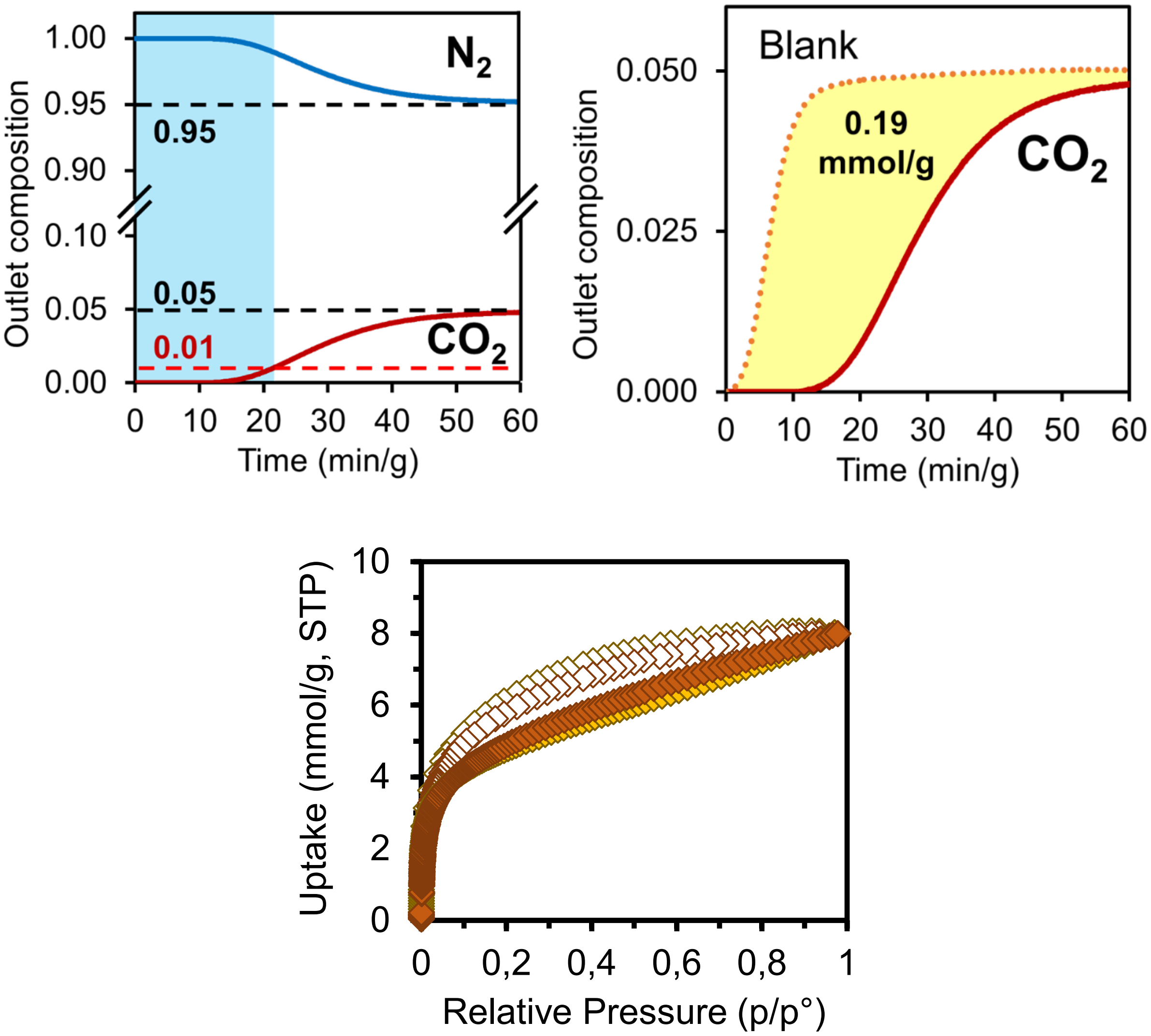

Figure S41. (Top, left) CO_2/N_2 (5/95) breakthrough curves measured with total flow rate of 4 sccm on **CXF1-OH** sample. (Top, right) CO_2 breakthrough curves compared with blank response: the yellow shaded area has been integrated to calculate the total amount of CO_2 adsorbed under dynamic conditions. The uptake of 0.19 mmol/g is in agreement with the pure CO_2 adsorption under same partial pressure and temperature conditions (0.20 mmol/g). (Down) CO_2 adsorption isotherms collected at 195 K and up to 1 bar for **CXF1-OH** (orange) and **CXF1-OH** after all adsorption experiments. Empty symbols define the desorption branch adsorption experiments.

17 CH_4 adsorption isotherms (CXF1-OMe and CXF1-OH)

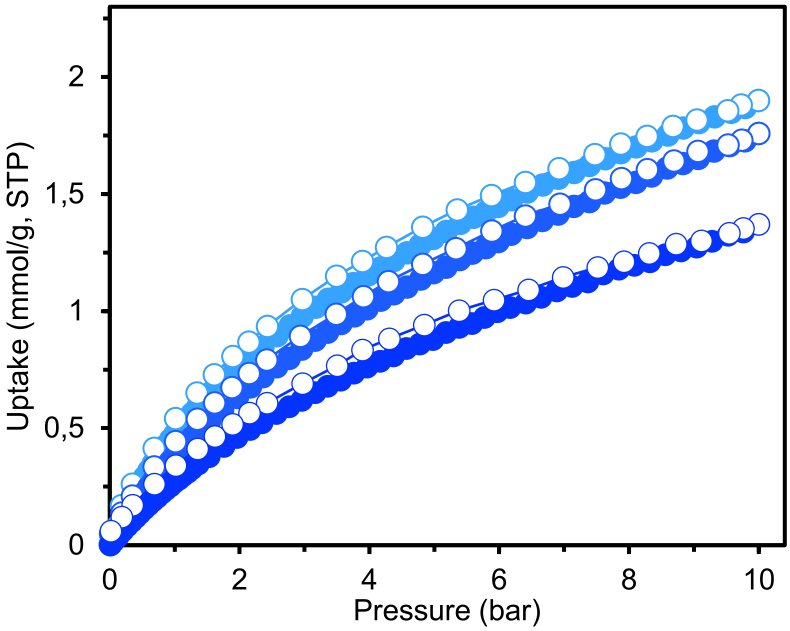

Figure S42. CH_4 adsorption isotherms of **CXF1-OMe** collected at 273 K (light blue), 283 K (blue) and 298 K (dark blue) up to 10 bar. Empty symbols define the desorption branch.

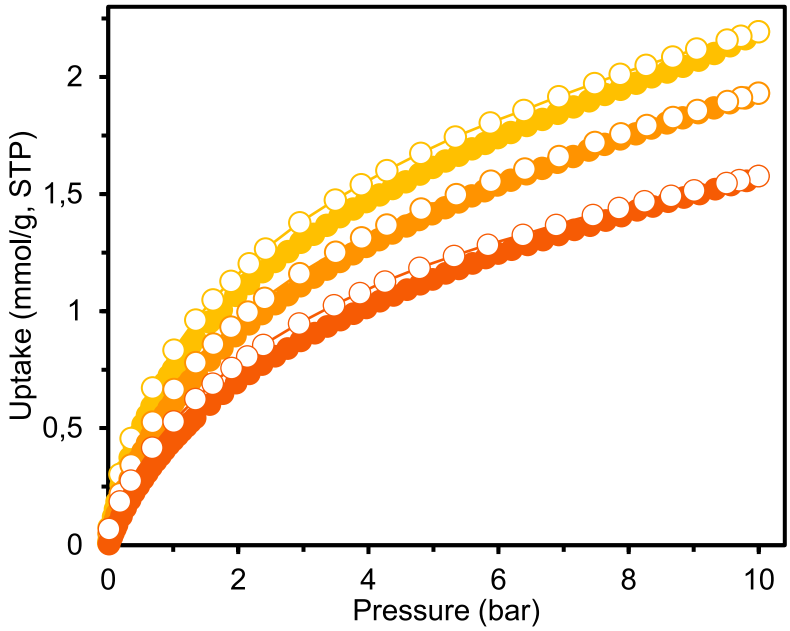

Figure S43. CH_4 adsorption isotherms of **CXF1-OH** collected at 273 K (light orange), 283 K (orange) and 298 K (dark orange) up to 10 bar. Empty symbols define the desorption branch.

The three isotherms, collected at 273 K, 283 K and 298 K up to 10 bar, were fitted adopting a dual-site Langmuir model (*eq. S2*) and $Q_{st}(CH_4)$ was derived using the van't Hoff equation (*eq. S1*). Calculations were run using Mathlab software: the calculated fitting parameters are reported in Table S9, while Figure S44 shows the fitted curve over the experimental isotherms.

Table S9. Fitting parameters obtained for methane adsorption for **CXF1-OMe** and **CXF1-OH** using a dual-site Langmuir model.

	$Q_{sat,A}$ (mmol/g)	$Q_{sat,B}$ (mmol/g)	$b_{0,A}$ (bar^{-1})	$b_{0,B}$ (bar^{-1})	E_A (kJ/mol)	E_B (kJ/mol)
CXF1-OMe	1.1117	8.3486	$2.00\cdot10^{-5}$	$2.92\cdot10^{-5}$	22.9642	13.949
CXF1-OH	1.5208	6.3734	$2.92\cdot10^{-5}$	$5.16\cdot10^{-5}$	32.5985	17.6361

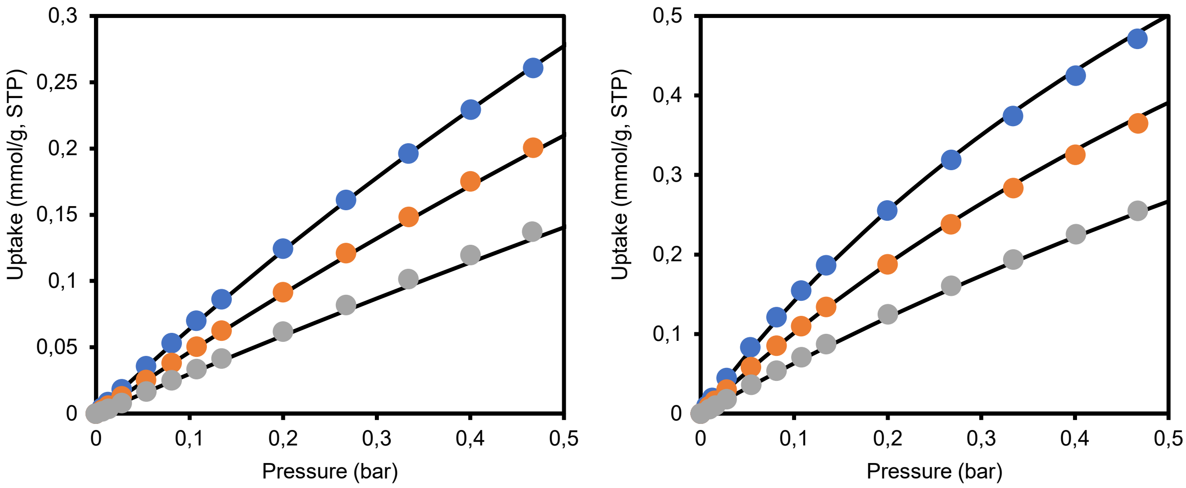

Figure S44. Fitting of CH_4 adsorption isotherms for **CXF1-OMe** (left) and **CXF1-OH** (right) using the parameters reported in Table X. CH_4 isotherms at 273 K (blue), 283 K (orange), 298 K (grey) and fittings (solid black trace) are reported.

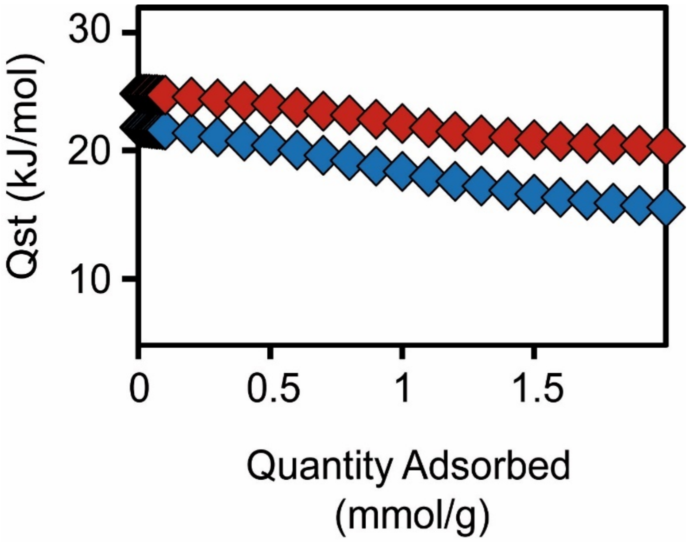

Figure S45. CH_4 heat of adsorption for **CXF1-OMe** (blue diamonds) and **CXF1-OH** (red diamonds).

Table S10. CH_4 adsorption capacities at 10 bar and 1 bar reported as mmol/g and wt %, isosteric heat for **CXFs**.

	T (K)	P (bar)	$Q_{10bar}(CH_4)$ (mmol/g)	(Q_{10bar}) wt%	$Q_{1bar}(CH_4)$ (mmol/g)	(Q_{1bar}) wt%	Q_{st}^{a} (kJ/mol)
CXF1-OMe	273	10	1.9	3.0	0.5	0.8	21
	283	10	1.7	2.7	0.4	0.6	
	298	10	1.4	2.2	0.3	0.5	
CXF1-OH	273	10	2.2	3.5	0.8	1.3	24
	283	10	1.9	3.0	0.6	1.0	
	298	10	1.6	2.6	0.4	0.6	

a)Calculated applying the van’t Hoff equation to the results of a fitting procedure of the experimental isotherms with a dual-site Langmuir model

18 CO_2 adsorption (co-CXFs)

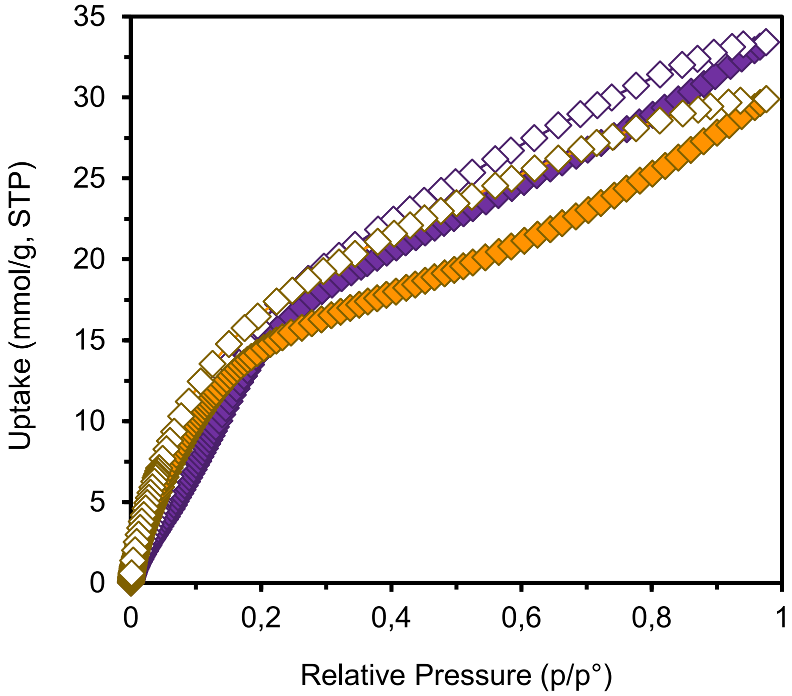

Figure S46. CO_2 adsorption isotherm collected at 195 K and up to 1 bar for **co-CXF3-OPr** (purple) and **co-CXF3-OH** (yellow). Empty symbols define the desorption branch.

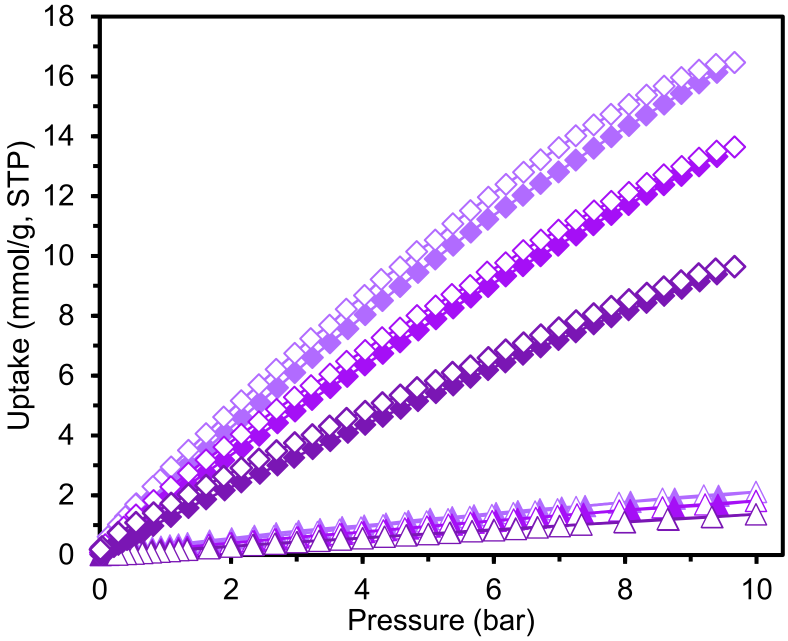

Figure S47. CO_2 (diamonds) and N_2 (triangles) adsorption isotherms of **co-CXF3-OPr** collected at 273 K (light purple), 283 K (purple) and 298 K (dark purple) up to 10 bar. Empty symbols define the desorption branch.

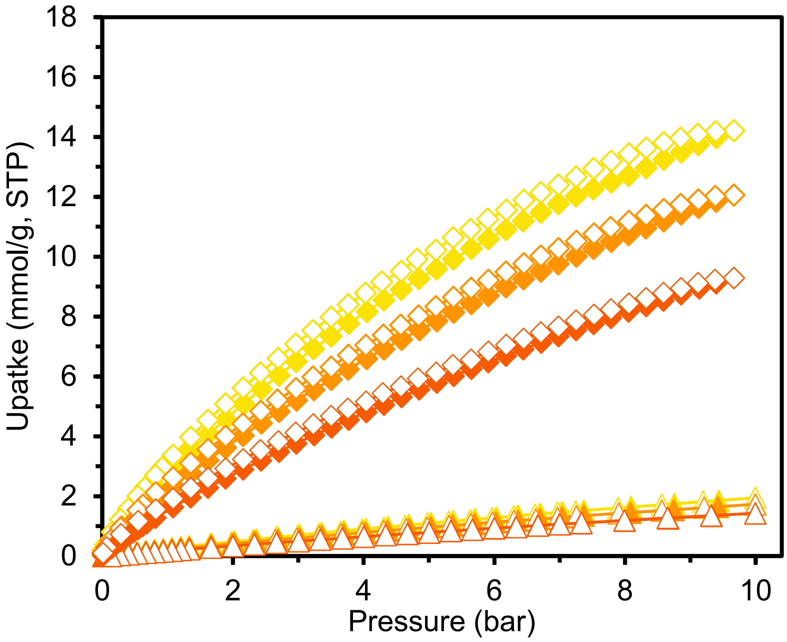

Figure S48. CO_2 (diamonds) and N_2 (triangles) adsorption isotherms of **co-CXF3-OH** collected at 273 K (yellow), 283 K (dark yellow) and 298 K (orange) up to 10 bar. Empty symbols define the desorption branch.

$Q_{st}(CO_2)$ was derived from CO_2 adsorption isotherms collected at 273 K, 283 K and 298 K up to 10 bar using the van't Hoff equation (*eq. S1*). The three isotherms were fitted adopting a Langmuir-Freundlich model, which has the general form

$$\boldsymbol{q} = \frac{q_{max} b p^t}{1+bp^t} \qquad (eq.\ S6)$$

where $\boldsymbol{q}$ is the adsorbed quantity at pressure p, q_{max} is the saturation loading and b and t are the Freundlich parameters. Parameter b can be written

$$b = b_0 e^{E/RT} \qquad (eq.\ S7)$$

where b_0 is a pre-exponential factor related to the gas saturation pressure $p°$ and E can be considered as the mean adsorbent-adsorptive interaction energy calculated from $p = 0$ to $p_{max.}$ The Langmuir-Freundlich model was used to fit simultaneously the three experimental curves. We allowed the saturation loading q_{max} and the Freundlich parameters t to vary independently for each curve, while the pre-exponential factor b_0 and the energy E were set to be the same for all the isotherms. Calculations were run using Mathlab software. The calculated fitting parameters are reported in Table

S11, while Figure S49 shows the fitted curve over the experimental isotherms. The Langmuir-Freundlich equation can be expressed as p *versus* $\boldsymbol{q}$,

$$p = \left(\frac{\boldsymbol{q}}{b(q_{max} - \boldsymbol{q})}\right)^{1/t} \qquad (eq.\ S8)$$

to calculate Q_{st} via the van't Hoff equation (*eq. S1*).

Table S11. Fitting parameters obtained for carbon dioxide adsorption for **co-CXFs** using a Langmuir-Freundlich model.

	Q_{273} (mmol/g)	Q_{283} (mmol/g)	Q_{298} (mmol/g)	t_{273}	t_{283}	t_{298}	b_0 (bar^{-1})	E (kJ/mol)
co-CXF3-OPr	76.7451	64.7203	48.4533	0.9468	0.9524	0.9672	$2.94 \cdot 10^{-3}$	5.3147
co-CXF3-OH	57.3781	49.0149	38.8003	0.8526	0.8693	0.8921	$3.90 \cdot 10^{-3}$	5.8087

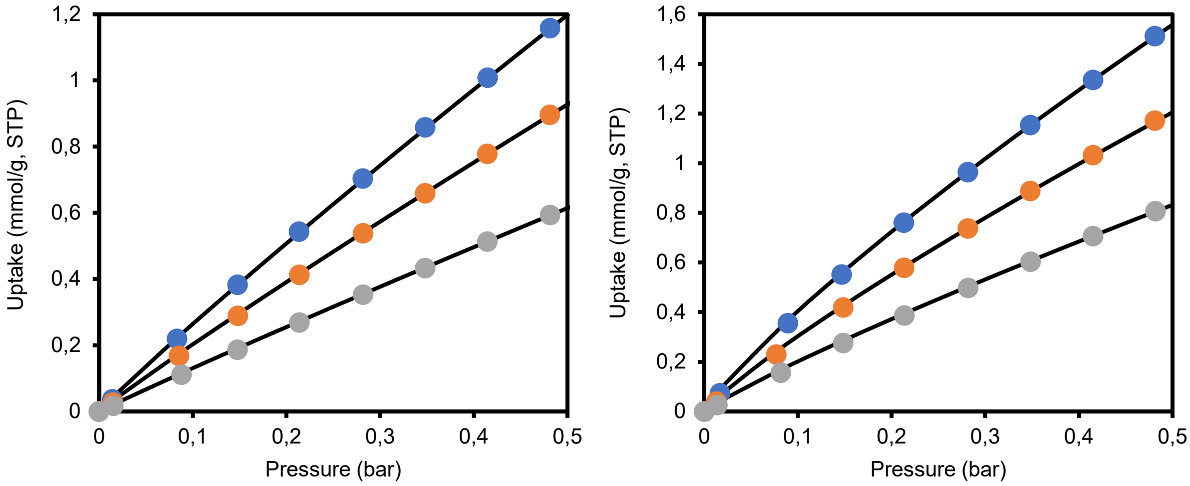

Figure S49. Fitting process for CO_2 adsorption isotherms of **co-CXF3-OPr** (left) and **co-CXF3-OH** (right) using the parameters reported in Table X. CO_2 isotherms at 273 K (blue), 283 K (orange), 298 K (grey) and fittings (solid black trace) are reported.

Table S12. CO_2 adsorption capacities at 10 and 1 bar reported as mmol/g and wt %, isosteric heat of adsorption calculated from adsorption data and CO_2/N_2 selectivities for **co-CXF3s**.

	T (K)	P (bar)	$Q_{10bar}(CO_2)$ (mmol/g)	(Q_{10bar}) wt%	$Q_{1bar}(CO_2)$ (mmol/g)	(Q_{1bar}) wt%	Q_{st}[b] (kJ/mol)
co-CXF3-OPr	195	1[a]	33.4	147.0	/	/	23.4
	273	10	16.5	72.6	2.4	10.6	
	283	10	13.6	59.9	1.9	8.4	
	298	10	9.6	42.2	1.3	5.7	
co-CXF3-OH	195	1[a]	29.1	128.1	/	/	30.0
	273	10	14.2	62.5	2.9	12.8	
	283	10	12.1	53.2	2.3	10.1	
	298	10	9.7	42.7	1.6	7.0	

[a] p/p^o is reported

[b] Calculated applying the van't Hoff equation to the results of a fitting procedure of the experimental isotherms with a Langmuir-Freundlich model

[c] low pressure value calculated applying the IAST theory to a 15:85 CO_2/N_2 mixture

19 CH_4 adsorption (co-CXFs)

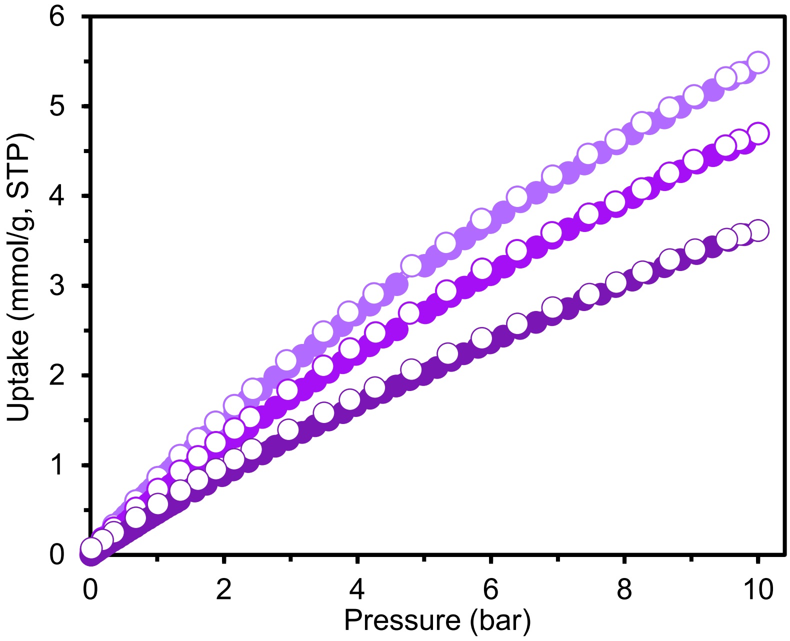

Figure S50. CH_4 adsorption isotherms of **co-CXF3-OPr** collected at 273 K (light purple), 283 K (purple) and 298 K (dark purple) up to 10 bar. Empty symbols define the desorption branch.

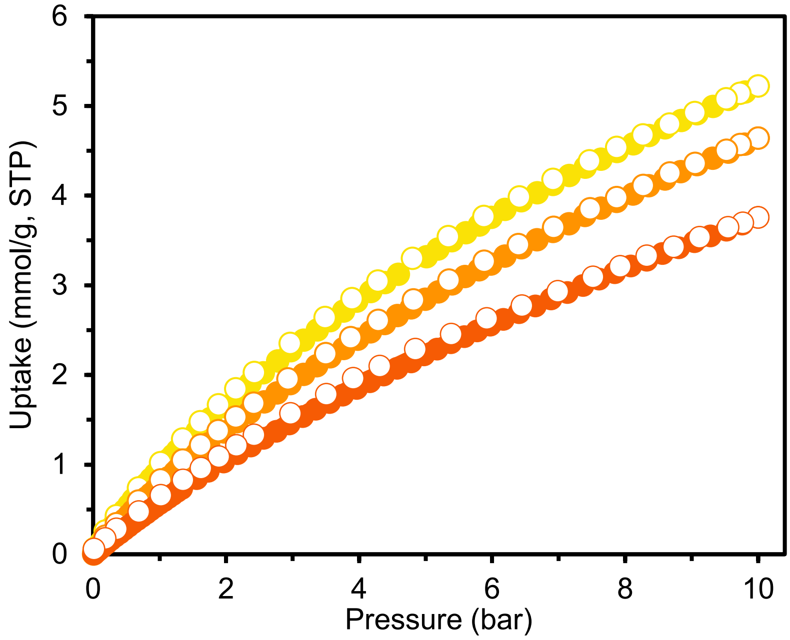

Figure S51. CH_4 adsorption isotherms of **co-CXF3-OH** collected at 273 K (yellow), 283 K (dark yellow) and 298 K (orange) up to 10 bar. Empty symbols define the desorption branch.

The three isotherms, collected at 273 K, 283 K and 298 K up to 10 bar of pressure, were fitted adopting a dual-site Langmuir model (*eq. S2*) and $Q_{st}(CH_4)$ was derived using the van't Hoff equation (*eq. S1*).

Calculations were run using Mathlab software: the calculated fitting parameters are reported in Table S13, while Figure S52 shows the fitted curve over the experimental isotherms.

Table S13. Fitting parameters obtained for methane adsorption for **co-CXF3s** using a dual-site Langmuir model.

	$Q_{sat,A}$ (mmol/g)	$Q_{sat,B}$ (mmol/g)	$b_{0,A}$ (bar^{-1})	$b_{0,B}$ (bar^{-1})	E_A (kJ/mol)	E_B (kJ/mol)
co-CXF3-OPr	6.2474	22.2160	$2.89\cdot10^{-6}$	$4.29\cdot10^{-5}$	18.0806	15.2336
co-CFX3-OH	1.0099	14.1302	$5.61\cdot10^{-6}$	$1.65\cdot10^{-4}$	26.0052	12.7247

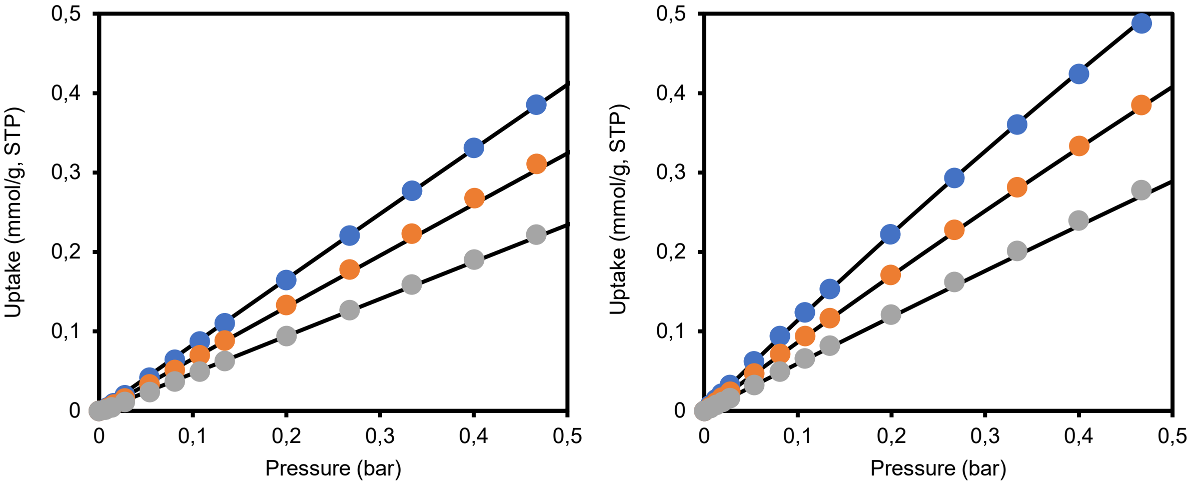

Figure S52. Fitting of adsorption isotherms for **co-CXF3-OPr** (left) and **co-CXF3-OH** (right) using the parameters reported in Table SX. CH_4 isotherms at 273 K (blue), 283 K (orange), 298 K (grey) and fittings (solid black trace) are reported.

Table S14. CH_4 adsorption capacities at 10 bar and 1 bar reported as mmol/g and wt % and isosteric heat for **co-CXFs**.

	T (K)	P (bar)	$Q_{10bar}(CH_4)$ (mmol/g)	(Q_{10ar}) wt%	$Q_{1bar}(CH_4)$ (mmol/g)	(Q_{1bar}) wt%	Q_{st}[a] (kJ/mol)
co-CXF3-OPr	273	10	5.5	8.8	0.8	1.3	15.4
	283	10	4.7	7.5	0.7	1.1	
	298	10	3.6	5.8	0.5	0.8	
co-CXF3-OH	273	10	5.2	8.3	1.0	1.6	18.0
	283	10	4.6	7.4	0.8	1.3	
	298	10	3.8	6.1	0.6	1.0	

[a] Calculated applying the van't Hoff equation to the results of a fitting procedure of the experimental isotherms with a dual-site Langmuir model

20. BET linear plots and BET surface area evaluation

BET surface areas were calculated according to the linear form of BET equation shown below:

$$\frac{p/p^\circ}{\boldsymbol{n}(1-p/p^\circ)} = \frac{1}{\boldsymbol{n}_m C} + \frac{(C-1)}{\boldsymbol{n}_m C}(p/p^\circ)$$

$\boldsymbol{n}$ is the specific amount of gas adsorbed

$\boldsymbol{n}_m$ is the monolayer capacity

C is the BET constant.

The BET surface area was then calculated taking into consideration the molecular cross-section of N_2 molecules (assuming it equal to 0.162 nm^2, as in close-packed liquid monolayer) according to the following equation:

$$S_{BET} = \boldsymbol{N_A} \boldsymbol{n}_m \sigma$$

$\boldsymbol{N_A}$ is the Avogadro constant

$\boldsymbol{n}_m$ is the monolayer capacity

σ is the molecular cross-section of nitrogen.

The BET equation was applied in the relative pressure range $0.015 < p/p^\circ < 0.1$. In this pressure range, the C constants were always positive and higher than 100 which is consistent with the formation of a monolayer below 0.1 p/p° (with the exception of material CXF3-OPr which does not show an appreciable nitrogen adsorption at 77 K (S_{BET} = 30 m^2/g).[7]

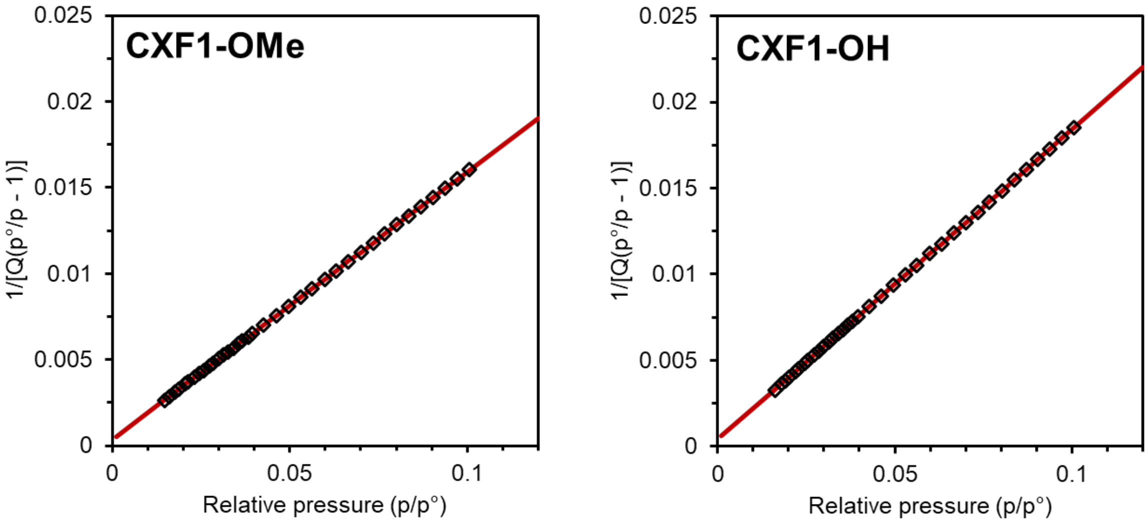

BET surface area:	626 m²/g
Slope:	0.155392 g/mmol
Y-intercept:	0.000374 g/mmol
C:	416.1
Qm:	6.42 mmol/g
Correlation coefficient:	0.999993
Molecular cross-sectional area:	0.1620 nm²

BET surface area:	540 m²/g
Slope:	0.180093 g/mmol
Y-intercept:	0.000403 g/mmol
C:	448.09
Qm:	5.54 mmol/g
Correlation coefficient:	0.9999963
Molecular cross-sectional area:	0.1620 nm²

Figure S53. BET linear plots, fitted curves and calculated parameters for compound **CXF1-OMe** and **CXF1-OH** between 0.015 and 0.1 p/p°.

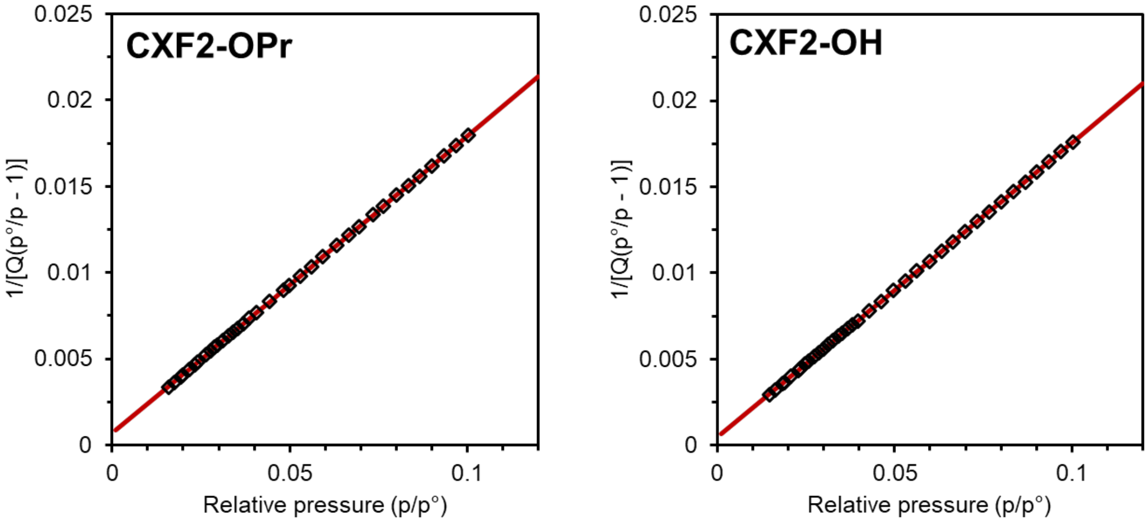

BET surface area:	564 m²/g
Slope:	0.172455 g/mmol
Y-intercept:	0.000672 g/mmol
C:	257.76
Qm:	5.78 mmol/g
Correlation coefficient:	0.999989
Molecular cross-sectional area:	0.1620 nm²

BET surface area:	569 m²/g
Slope:	0.170915 g/mmol
Y-intercept:	0.000469 g/mmol
C:	365.8
Qm:	5.83 mmol/g
Correlation coefficient:	0.999993
Molecular cross-sectional area:	0.1620 nm²

Figure S54. BET linear plots, fitted curves and calculated parameters for compound **CXF2-OPr** and **CXF2-OH** between 0.015 and 0.1 p/p°.

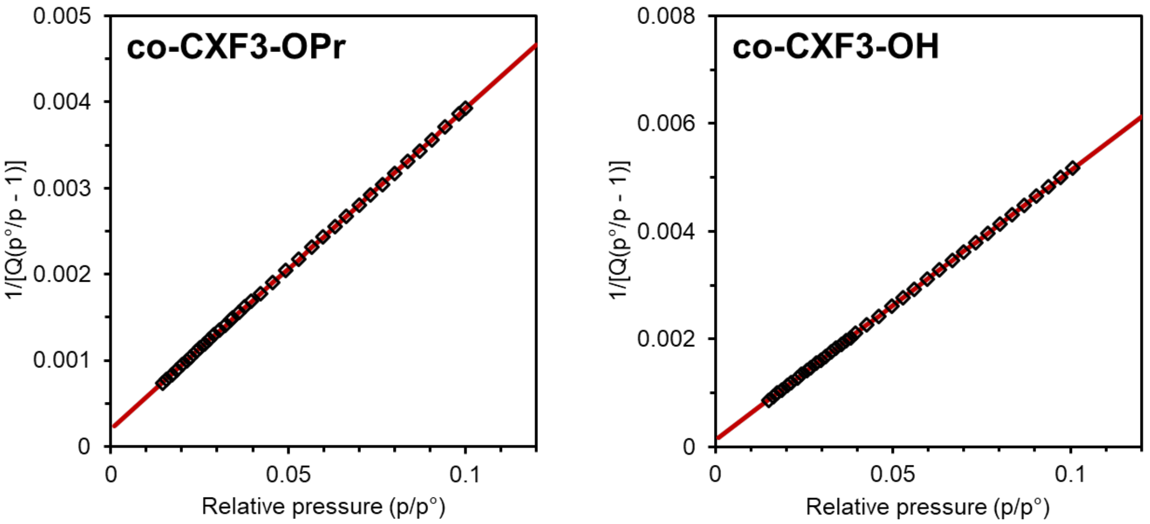

BET surface area:	2609 m²/g
Slope:	0.037176 g/mmol
Y-intercept:	0.000204 g/mmol
C:	183.15
Qm:	26.75 mmol/g
Correlation coefficient:	0.999973
Molecular cross-sectional area:	0.1620 nm²

BET surface area:	1943 m²/g
Slope:	0.050078 g/mmol
Y-intercept:	0.000121 g/mmol
C:	414.9
Qm:	19.92 mmol/g
Correlation coefficient:	0.999993
Molecular cross-sectional area:	0.1620 nm²

Figure S55. BET linear plots, fitted curves and calculated parameters for compound **co-CXF3-OPr** and **co-CXF3-OH** calculated between 0.015 and 0.1 p/p°.

21 References

(1) Läppchen, T.; Dings, R. P. M.; Rossin, R.; Simon, J. F.; Visser, T. J.; Bakker, M.; Walhe, P.; Van Mourik, T.; Donato, K.; Van Beijnum, J. R.; Griffioen, A. W.; Lub, J.; Robillard, M. S.; Mayo, K. H.; Grüll, H. *Eur. J. Med. Chem.* **2015**, *89*, 279.

(2) Casnati, A.; Pirondini, L.; Pelizzi, N.; Ungaro, R. *Supramol. Chem.* **2000**, *12* (1), 53.

(3) Soi, A.; Bauer, W.; Mauser, H.; Moll, C.; Hampel, F.; Hirsch, A. *J. Chem. Soc. Perkin Trans. 2* **1998**, No. 6, 1471.

(4) Mendez-Arroyo, J.; Barroso-Flores, J.; Lifschitz, A. M.; Sarjeant, A. A.; Stern, C. L.; Mirkin, C. A. *J. Am. Chem. Soc.* **2014**, *136* (29), 10340.

(5) Rathore, R.; Abdelwahed, S. H.; Guzei, I. A. *J. Am. Chem. Soc.* **2004**, *126* (42), 13582.

(6) Feldmann, W.-K.; White, K.-A.; Bezuidenhout, C. X.; Smith, V. J; Esterhuysen, C.; Barbour, L.J. *ChemSusChem.* **2020**, *13*, 102. Perego, J.; Bezuidenhout, C. X.; Pedrini, A.; Bracco, S.; Negroni, M.; Comotti, A.; Sozzani P. *J. Mater. Chem. A* **2020**, *8*, 11406.

(7) F. Rouquerol, J. Rouquerol and K. Sing in *Adsorption by powders and porous solids, Principles, Methodology and Applications*. Acad. Press. (Copyright 1999), (II Edition).